Observations of nonlinear momentum fluxes over the inner continental shelf

Thomas P. Connolly[1] and Steven J. Lentz[2]

[1]Moss Landing Marine Laboratories

San José State University

8272 Moss Landing Rd., Moss Landing, CA, 95039

tconnolly@mlml.calstate.edu (corresponding author)

[2]Department of Physical Oceanography

Woods Hole Oceanographic Institution

266 Woods Hole Road, MS 21, Woods Hole, MA, 02543

slentz@whoi.edu

June 1, 2020

ABSTRACT

Nonlinear momentum fluxes over the inner continental shelf are examined using moored observations from multiple years at two different locations in the Middle Atlantic Bight. Inner shelf dynamics are often described in terms of a linear alongshore momentum balance, dominated by frictional stresses generated at the surface and bottom. In this study, observations over the North Carolina inner shelf show that the divergence of the cross-shelf flux of alongshore momentum is often substantial relative to the wind stress during periods of strong stratification. During upwelling at this location, offshore fluxes of alongshore momentum in the surface layer partially balance the wind stress and reduce the role of the bottom stress. During downwelling, onshore fluxes of alongshore momentum reinforce the wind stress and increase the role of bottom stress. Over the New England inner shelf, nonlinear terms have less of an impact in the momentum balance and exhibit different relationships with the wind forcing. Differences between locations and time periods are explained by variations in bottom slope, latitude, vertical shear and cross-shelf exchange. Over the New England inner shelf, where moored density data are available, variations in vertical shear are explained by a combination of thermal wind balance and wind stress. An implication of this study is that cross-shelf winds can potentially influence the alongshore momentum balance over the inner shelf, in contrast with deeper locations over the middle to outer shelf.

Keywords— Momentum balance, Nonlinear, Momentum flux, Coastal dynamics, Upwelling dynamics, Downwelling dynamics, Thermal wind balance, Inner shelf

1. Introduction

The dynamics of the inner continental shelf govern exchange between shallower waters in the surf zone and deeper waters over the middle to outer shelf. The inner shelf is often dynamically defined as a region where the surface and bottom boundary layers interact and turbulent stresses are present throughout the entire water column (Mitchum and Clarke, 1986; Lentz, 1995; Lentz and Fewings, 2012). The inner shelf region is also characterized by cross-shelf mass transport that is reduced from the theoretical Ekman transport expected for deeper water (Lentz et al., 1999; Kirincich et al., 2005). The offshore extent of the inner shelf is strongly influenced by stratification, which inhibits turbulent mixing and restricts the region of reduced cross-shelf transport to shallower depths (Lentz et al., 1999). Unlike the middle to outer shelf, cross-shelf winds often drive significant transport and influence turbulent mixing over the inner shelf (Tilburg, 2003; Fewings et al., 2008; Horwitz and Lentz, 2014). Tidal currents are also expected to strongly influence vertical mixing over the inner shelf (Castelao et al., 2010). In the unique dynamical regime of the inner shelf, cross-shelf exchange is part of a complex set of interactions between wind forcing, stratification, density fronts and boundary-layer turbulence.

The alongshore momentum balance is frequently used as a framework for understanding the dynamics of coastal regions, including the inner shelf. The depth-averaged balance over the inner shelf is often characterized as being dominated by the frictional terms, wind stress and bottom stress, with secondary contributions from local acceleration and alongshore pressure gradients (Hickey, 1989; Lentz et al., 1999; Lentz and Fewings, 2012). In addition to bottom stress, the alongshore pressure gradient has also been shown to be important in balancing the wind stress at some locations, particularly at locations near alongshore variations in bathymetry and coastline (Kirincich and Barth, 2009b; Fewings and Lentz, 2010). However, the potential impact of additional nonlinear terms in the depth-averaged alongshore momentum balance is not well known and is often neglected for simplicity (Lentz and Fewings, 2012). Nonlinear terms are also often neglected when

the momentum balance is evaluated over a portion of the water column rather than the depth average (Lentz, 2001). If nonlinear terms are significant, neglecting them could lead to misinterpretation of the magnitude of stresses at the bottom or in the interior of the water column, which are often uncertain or unknown. The goal of this study is to assess the importance of nonlinear momentum fluxes in observations at different locations, and provide a mechanistic understanding of how they arise in response to wind forcing over the inner shelf.

In deeper water over the middle to outer shelf, nonlinear momentum fluxes have been found to strongly influence upwelling dynamics under certain conditions. Lentz and Chapman (2004) show that the divergence of the cross-shelf flux of alongshore momentum is important in balancing upwelling-favorable alongshore wind stress over continental shelves characterized by strong stratification and a steep bottom slope. At locations with strong stratification and steep bottom slope, the role of bottom friction is reduced and the onshore return flow occurs in the geostrophic interior region between the turbulent boundary layers, rather than in the bottom boundary layer. Theory also predicts that cross-shelf momentum flux divergence reinforces the wind stress during downwelling-favorable wind forcing, allowing for the magnitude of the bottom stress to exceed that of the wind stress (Lentz and Chapman, 2004). The role of the nonlinear momentum flux divergence is unclear over the inner shelf where the boundary layers interact, there is no distinct geostrophic interior region and cross-shore wind stress can be an important part of the forcing.

Previous studies that have taken nonlinear terms into account over the inner shelf have focused on a range of different mechanisms and have reached different conclusions about the importance of nonlinear processes. In Monterey Bay on the central California coast, Woodson (2013) found that nonlinear interaction between offshore surface transport and relative vorticity associated with the alongshore flow can be important in balancing wind stress in the surface layer, along with the Coriolis force. These observations, combined

with high levels of stratification and shallow estimates of the boundary layer thickness, suggest that the reduction of surface transport from theoretical Ekman transport is not necessarily associated with significant stress at the base of the surface layer. Over the Oregon inner shelf, Kirincich and Barth (2009b) found the divergence of the cross-shelf flux of along-shelf momentum to be important in balancing the wind stress. The presence of strong vertical shear in these observations indicates that the mechanism is similar to that described by Lentz and Chapman (2004) for mid-shelf locations, although the importance of the nonlinear term over the Oregon inner shelf varies at different sites along the same isobath with similar stratification and bottom slope. Estimates of this nonlinear term are also substantial relative to the wind stress during periods of strong stratification over the Catalan inner shelf in the Mediterranean (Grifoll et al., 2012). However, numerical modeling over the West Florida shelf indicates that the nonlinear terms are small, consistent with a linear balance (Liu and Weisberg, 2005). Observations from a range of different locations, and subject to a range of different forcing conditions, are needed to clarify the role of this nonlinear process over the inner shelf.

This study assesses the role of nonlinear momentum fluxes in the alongshore momentum balance at two different inner shelf locations in the Middle Atlantic Bight: the Martha's Vineyard Coastal Observatory (MVCO) over the New England inner shelf and the Army Corps of Engineers Field Research Facility (FRF) over the North Carolina inner shelf (Fig. 1). Because of differences in latitude and coastline orientation, these two locations are subject to different seasonal variations in wind forcing, but a strong cross-shelf component of wind stress is present at both locations (Lentz, 2008a). Tidal current amplitudes decrease from $\sim$0.3 m/s near MVCO to $<$0.1 m/s near FRF (Moody et al., 1984). At MVCO, the alongshore momentum balance has primarily been examined in a linearized framework, and a dominant balance between the wind stress and alongshore pressure gradient has been observed (Fewings and Lentz, 2010). At FRF, Lentz et al. (1999) also examined a linearized momentum balance and identified a dominant balance between the

wind stress and bottom stress. Nonlinear terms have also been neglected in the alongshore momentum balance integrated over the surface layer at this site (Lentz, 2001). However, two dimensional numerical modeling suggests that nonlinear momentum fluxes strongly influence the alongshore momentum balance at FRF, playing a major role in balancing the wind stress during upwelling and a more minor role in reinforcing the wind stress during downwelling (Kuebel Cervantes et al., 2003; 2004). In the present study, observations from both sites are compared under a range of forcing conditions to assess the importance of the nonlinear terms and identify physical mechanisms that determine how and when they become important.

At each location, data from long-term current meter arrays are used to evaluate the importance of the nonlinear terms in alongshore momentum balances. In Section 2, alongshore momentum balance equations are presented in two forms, both depth-averaged and integrated over the surface layer. These momentum balances assume a two-dimensional mass balance, but account for important effects of surface gravity waves over the inner shelf and include the divergence of the cross-shelf flux of alongshore momentum. Observations and methods for estimating terms of the momentum balance are presented in Section 3. Descriptive overviews of the MVCO and FRF observations are provided (Section 4.a), before presenting analyses of the depth-averaged and surface-integrated momentum balances (Sections 4.b,c). Processes influencing vertical shear, an important component of the nonlinear momentum flux divergence, are evaluated using moored density time series observations at MVCO (Section 4.d). As discussed in Section 5, it is found that the contrasting patterns of wind forcing and cross-shelf exchange at MVCO and FRF lead to different relationships between the alongshore wind stress and the momentum flux divergence. The importance of the nonlinear momentum flux divergence also differs between these two sites. Variations in the magnitude of the nonlinear term relative to the wind stress are determined by a combination of bottom slope, vertical shear, the Coriolis parameter, and the fraction of cross-shelf surface transport relative to the deep water Ekman

transport. Major implications of this work are that 1) the vertical shear of the alongshore current is a key parameter in inner shelf dynamics, and 2) cross-shelf wind stress has the potential to influence the alongshore momentum balance over the inner shelf.

2. Alongshore momentum balances

To provide a theoretical framework for the analysis, simplified alongshore momentum balances are developed for the inner continental shelf. The primary purpose of the momentum balance analysis is to assess the importance of the cross-shelf momentum flux divergence. A major simplification is the assumption of a two-dimensional mass balance, neglecting alongshore variations in currents and the surface gravity wave field. There is evidence for this type of mass balance at both inner-shelf locations examined in this study when the effects of wave-driven transport are included (Lentz et al., 2008). However, this assumption would not be valid in locations where alongshore variations in topography are present over short scales and alongshore advection of momentum can be important in balancing localized pressure gradients (e.g. Ofsthun et al., 2019). The effects of wave breaking in the surf zone are also not included in the analysis, which focuses on the inner shelf region offshore of the surf zone.

The effects of unbroken surface gravity waves over the inner shelf are accounted for by considering the wave-averaged Lagrangian cross-shelf velocity $\mathbf{u}_L = \mathbf{u} + \mathbf{u}_{st}$, where $\mathbf{u}$ is the wave-averaged Eulerian velocity vector and $\mathbf{u}_{st}$ is the Stokes drift vector. Wave-averaged observations collected by a current meter at a fixed location represent only the Eulerian component $\mathbf{u}$, but $\mathbf{u}_{st}$ also contributes to additional transport of mass and tracers in the direction of wave propagation (Monismith and Fong, 2004). The presence of the Stokes drift, $\mathbf{u}_{st}$, influences the alongshore momentum balance through the Stokes-Coriolis force (Xu and Bowen, 1994; Lentz et al., 2008) and vortex force terms (Smith, 2006; Uchiyama et al., 2010).

a. Depth-averaged momentum balance

As a starting point for developing a simplified two-dimensional momentum balance for the inner shelf, a three-dimensional balance that includes the effects of wave breaking is first considered. The x coordinate is defined as positive offshore, and the y coordinate is oriented alongshore (Fig. 1b,c). Following Uchiyama et al. (2010), a depth-averaged alongshore momentum balance that includes the effects of both breaking and unbroken surface waves can be written in a flux-divergence form,

$$\frac{\partial \bar{v}}{\partial t} + \frac{1}{D}\frac{\partial}{\partial x}\int_{-h}^{\eta}(u_L v)\,dz + \frac{1}{D}\frac{\partial}{\partial y}\int_{-h}^{\eta}(v_L v)\,dz - \left(\overline{u_{st}\frac{\partial u}{\partial y}}\right) - \left(\overline{v_{st}\frac{\partial v}{\partial y}}\right) = -\frac{1}{\rho_o}\frac{\partial \overline{p}}{\partial y} - f\bar{u}_L + \frac{\tau^{sy}}{\rho_o D} - \frac{\tau^{by}}{\rho_o D} + \frac{\epsilon k^y}{\rho_o D\sigma} \quad (1)$$

where η is sea level, h is bottom depth, $D = \eta + h$ is the total thickness of the water column, ρ_o = 1025 kg/m^3 is a constant reference density, f is the Coriolis parameter, τ^{sy} is the alongshore component of surface wind stress, τ^{by} is the alongshore component of bottom stress, ϵ is the wave dissipation rate, k^y is the alongshore component of the wavenumber, and σ is the wave frequency. Overbars indicate depth-averaged quantities, for example,

$$\bar{v} = \frac{1}{D}\int_{-h}^{\eta} v\,dz. \quad (2)$$

Assuming a two-dimensional mass balance ($\bar{u}_L = 0$), neglecting the effects of wave dissipation outside of the surf zone, and neglecting alongshore variations in currents and waves, the alongshore momentum balance in equation (1) can be simplified as

$$\frac{\partial \bar{v}}{\partial t} + \frac{1}{D}\frac{\partial}{\partial x}\int_{-h}^{\eta}(u_L v)\,dz = -\frac{1}{\rho_o}\frac{\partial \overline{p}}{\partial y} + \frac{\tau^{sy}}{\rho_o D} - \frac{\tau^{by}}{\rho_o D}. \quad (3)$$

The left-hand side of equation (3) includes local acceleration and the nonlinear momentum

flux divergence term. This nonlinear term combines the effects of 1) nonlinear advection of alongshore momentum by the cross-shore Eulerian circulation, and 2) the vortex force induced by the interaction of the cross-shelf component of Stokes drift and the alongshore current. Model results show that Eulerian advection and vortex force terms are often substantial, but tend to offset each other in the depth-averaged balance (Uchiyama et al., 2010; Kumar et al., 2012). To assess their net impact on the dynamical balance these two effects are combined into a single nonlinear term, which represents the divergence of the cross-shore flux of alongshore momentum. This term is potentially significant if there is cross-shelf exchange ($u_L \neq 0$), vertical shear in the alongshore current is present ($\partial v/\partial z \neq 0$), and cross-shelf variations exist ($\partial/\partial x \neq 0$). The nonlinear term is present in this simplified two-dimensional framework, but it is not present in one-dimensional models of the water column.

The right-hand side of the simplified momentum balance in equation (3) contains the alongshore pressure gradient, surface stress and bottom stress terms which have been demonstrated as dynamically important in previous studies (Lentz et al., 1999; Fewings and Lentz, 2010). The present study primarily uses information from cross-shelf current meter arrays deployed over multiple years at two different inner shelf locations. Although data are not available to accurately estimate the alongshore pressure gradient term, the current meter data allow for estimates of the nonlinear term. Estimates of the nonlinear term are compared with estimates of surface and bottom stresses, and the importance of the nonlinear term is assessed under different wind forcing and stratification conditions.

b. Surface layer momentum balance

The alongshore momentum balance is also analyzed over a portion of the water column near the surface in order to relate the nonlinear dynamics to cross-shelf exchange and turbulent stresses. Cross-shore surface transport U_S is calculated from the vertical integral of the Lagrangian cross-shelf velocity in the upper layer of the water column

$$U_S = \int_{z_s}^{\eta} u_L \, dz, \tag{4}$$

where z_s is the depth of the first zero crossing in the vertical profile of u_L. The terms in the alongshore momentum balance are integrated over this same surface layer.

Consistent with the depth-averaged balance described above in Section 2.a, the surface layer momentum balance considered in this study neglects alongshore variations in currents and waves, as well as wave dissipation in the surf zone. The alongshore momentum balance integrated over the upper layer is given by

$$\frac{\partial}{\partial t}\int_{z_s}^{\eta} v \, dz + \frac{\partial}{\partial x}\int_{z_s}^{\eta} (u_L v) \; dz - (w_L v)|_{z=z_s} = -\frac{1}{\rho_o}\int_{z_s}^{\eta} \frac{\partial p}{\partial y} \, dz - f U_s + \frac{\tau^{sy}}{\rho_o} - \frac{\tau^{iy}}{\rho_o}|_{z=z_s} \tag{5}$$

where w_L is the Lagrangian vertical velocity and $\tau^{iy}|_{z=z_s}$ is the interior turbulent stress at the base of the surface layer. The Lagrangian vertical velocity at the base of the surface layer can be determined from conservation of volume,

$$w_L|_{z=z_s} = \frac{\partial \eta}{\partial t} + \frac{\partial U_s}{\partial x}. \tag{6}$$

Like the depth-averaged momentum balance, the left hand side of the surface layer momentum balance in equation (5) contains a local acceleration term in addition to nonlinear terms. The two nonlinear terms represent the net flux of alongshore momentum into the surface layer at a given cross-shelf location. Both the cross-shore and vertical components of the Lagrangian velocity $\mathbf{u}_L$ contribute to the flux of alongshore momentum into the surface layer. Both of these terms are dependent on cross-shore variations ($\partial/\partial x$) and cannot exist in one-dimensional models of the water column, even those with sophisticated turbulence closure schemes. The right-hand side of equation (5) contains the alongshore pressure gradient, Coriolis force, surface stress and interior stress at the base of the surface layer. This study focuses on comparing the wind stress, Coriolis and nonlinear terms. Al-

217 though direct observations of interior stresses are not available in this study, implications
218 of the results for turbulent stresses over the inner shelf will be discussed.

219 3. Methods

220 *a. Data sources*

221 To address the role of nonlinear terms in the momentum balance, this study uses
222 observations from Duck, NC, and Martha's Vineyard, MA (Fig. 1). At both of these sites,
223 velocity data are available for several years at multiple cross-shelf locations.

224 *i. Duck, NC* A long-term array of five acoustic current profilers at bottom depths of
225 5-11 m, was maintained by the Army Corps of Engineers Field Research Facility (FRF)
226 at Duck, North Carolina (Fig. 1b). Velocity data from the time period November 2008
227 to July 2014 are used in this study. These data are publicly available on the FRF data
228 portal. At the 5, 6, 8 and 11m sites, Nortek Acoustic Wave and Current (AWAC) profilers
229 obtain velocity profiles with vertical resolution of 0.5 m. The bottom velocity bins are
230 located 1.5m above the bottom at the 5 and 6m sites and 1.0m above the bottom at the
231 8 and 11m sites. The AWAC profilers also obtain measurements of surface gravity wave
232 characteristics, including significant wave height (H_{sig}), peak period and direction.

233 Stokes drift profiles, $\mathbf{u}_{st}$, and depth averages, $\bar{\mathbf{u}}_{st}$, are computed from observed bulk
234 wave characteristics (H_{sig}, peak period, direction) following Lentz et al. (2008). Time pe-
235 riods when sites are in the surf zone are excluded from the analysis based on a conservative
236 criterion of $H_{sig} < 0.33h$. When wave data are not available at a site, wave height and
237 period from the nearest available site are used and direction is calculated from the nearest
238 available site using Snell's law. Remaining short gaps of up to 6 hours in $\mathbf{u}_{st}$ and $\bar{\mathbf{u}}_{st}$ are
239 filled using linear interpolation. Gaps of the same size in the FRF ADCP velocities are
240 filled by first removing tidal velocities, linearly interpolating over the gaps, then adding
241 back the tidal velocities. The tidal analysis is performed using a Python distribution of
242 UTide (Codiga, 2011), using tidal constituents with periods of less than 48 hours. At each

site, all current and Stokes drift vectors are rotated so that the y axis is aligned with principal axis of $\bar{\mathbf{u}}_L$. The principal axis angles vary between 18.4-21.6° counter-clockwise from true north.

In addition to the long-term current meter array, conductivity, temperature and depth (CTD) profiles are collected on a nominal daily basis from the end of a pier at FRF (Fig. 1b). These data are used to provide information on water column stratification. Profiles of water column temperature and practical salinity are available through the FRF data portal. Wind speed and direction at the FRF site are measured by an anemometer at a height of 16.4 m above the water at the end of the FRF pier (NDBC station DUKN7). Wind vectors at FRF are rotated into a coordinate system in which the y axis is 20° clockwise from true north. Meteorological data were obtained from the National Data Buoy Center (NDBC).

Nearshore bathymetry data (Fig. 1b) near Duck, NC were collected by Dr. Jesse McNinch and are available in Thieler et al. (2013). Nearshore bathymetry data used for depths 2.5-9 m are gridded at 10-m horizontal resolution; data used for depths 10 m and greater are gridded at 40-m horizontal resolution. Regional-scale bathymetry data on a 30 arc-second grid were obtained from the General Bathymetric Chart of the Oceans GEBCO_2014 Grid, version 20150318 (http://www.gebco.net, Fig. 1a).

ii. Martha's Vineyard, MA As part of the Stratification, Wind, and Waves on the Inner shelf of Martha's Vineyard (SWWIM) field program, an array of moorings was deployed during the time period from October 2006 to February 2010. The cross-shelf array consisted of four sites ranging in depth from 7 m to 27 m. A description of the complete data set is given by Horwitz and Lentz (2016), and a brief summary of the relevant data is provided here.

To facilitate comparison with the data from FRF, where the deepest site is at 11 m, this study focuses on the two inshore SWWIM sites at 7 m and 12 m (Fig. 1c). Velocity data from the 7-m site were obtained from an upward-looking 1200 kHz ADCP. Vertical bins used for analysis span heights from 1.75 m above the bottom to within 0.75 m from

the surface, with 0.25 m vertical spacing. Data were collected at 1 Hz in 6.7 min or 9 min bursts and averaged every 20 min. At the 12-m site, a 1200-kHz ADCP collected data at a cabled node of the MVCO. Vertical bins used for analysis span heights from 2.5 m above the bottom to within 2.5 m below the surface, with 0.5 m vertical spacing. Data were collected at 2 Hz and averaged into 20 min ensembles. The ADCP data at the 12-m site are also used to compute wave characteristics, including H_{sig}, peak period and direction. Stokes drift is calculated in the same manner as the FRF data. In the SWWIM data, where tidal velocities account for a greater fraction of the variance, a more restrictive threshold of 1 hour is used for linear interpolation of gaps. Principal axis angles in the SWWIM data are computed from $\bar{\mathbf{u}}$ during time periods when waves are relatively small ($H_{sig} < 0.75$) following Lentz et al. (2008).

In addition to velocity, time series of seawater density and wind are used at this site. Seawater density is calculated from temperature and conductivity data collected at the 7 m and 12 m sites using SBE-37 MicroCATs spaced at 2 m intervals throughout the water column. Wind speed and direction data are obtained from the MVCO beach meteorological mast, at a height 12 m above the surface. The wind data are rotated into the same coordinate system defined by principal axis of the 12-m site.

b. Estimates of momentum balance terms

The focus of this study is assessing the importance of the nonlinear terms in the momentum balances in equations (3) and (5). Since the nonlinear terms contain derivatives in the cross-shore direction, mooring data from two adjacent sites at different bottom depths are used to estimate this term. Vertical integrals of $(u_L v)$ are estimated at the inshore and offshore sites before taking their difference. The average of the two bottom depths is used for D. Where sufficient data are available, estimates of additional terms are averaged between the same two sites. At the FRF site, the momentum balance analysis focuses on the 6 m and 8 m sites due to availability of overlapping ADCP data. At the MVCO site, analysis focuses on data from the 7 m and 12 m sites.

Vertical integrals involving ADCP data, such as the depth integral of v in equation (2), are estimated using the trapezoidal rule. Velocity is linearly interpolated from the bottom bin to zero at the seabed and extended from the top bin upward to the sea surface. The depth-averaged cross-shelf velocity $\bar{u}_L$ is subtracted from the cross-shelf velocity profile before estimating vertical integrals of u_L and $(u_L v)$, which enforces a two-dimensional mass balance in which the net surface transport is zero. This isolates the depth-dependent circulation associated with wind-driven upwelling and downwelling, and is consistent with previous studies of the cross-shelf circulation at FRF and MVCO (Lentz, 2001; Fewings et al., 2008). In calculating the surface transport U_s (equation 4), the depth of the first zero crossing, z_s, in the vertical profile of u_L is estimated using linear interpolation. The vertical component of Lagrangian velocity, w_L in equation (6), is estimated using the difference between U_s at the two stations. The contribution of the temporal derivative in sea surface height was found to be negligible in the calculation of w_L and is neglected. To estimate the vertical momentum flux term in equation (5), values of v are interpolated to the zero crossing depth z_s at each station and averaged. Time derivatives of local acceleration are estimated using a center difference method. Estimates of momentum balance terms are made from unfiltered (20 minute or hourly) data, then low-pass filtered to focus on subtidal time scales. Low pass filtered quantities are computed using a PL64 filter with a half-amplitude period of 33 hours (Rosenfeld, 1983).

Estimates of the nonlinear term at FRF are further restricted to time periods when the assumption of two dimensional mass balance is justified. We restrict analysis of the FRF data to time periods when the magnitude of the depth averaged cross-shelf velocity $|\bar{u}_L| <$ 0.03 m/s. The magnitude of $\bar{u}_L$ exceeds this threshold 3-8% of the time at the different sites at FRF. This does not occur during June–August at the 6m or 8m sites, where much of the detailed analysis is focused. Restricting the analysis to times when $|\bar{u}_L| < 0.03$ m/s excludes the effects of three-dimensional processes which could be important in the momentum balance but cannot be evaluated with the cross-shelf mooring arrays used in

this study.

Surface and bottom stress estimates are made using bulk formulas. Wind stress is computed using the quadratic drag coefficient formulation of Smith (1988). Two different formulations are used to estimate bottom stress from the ADCP observations at the FRF site. First, a quadratic drag law is used, assuming a logarithmic boundary layer. The roughness length, z_o is estimated from $z_o = k_s/30$, where k_s is a grain roughness. The grain roughness is computed as $k_s = 2.5D$, using the median grain size D = 0.017 cm at Duck, NC (Lee et al., 2002). In terms of a drag coefficient $C_D = [\kappa/\ln(z/z_o)]^2$, where κ is Von Karman's constant, the resulting value of $z_o = 1.4\times10^{-5}$ m corresponds to $C_D = 1.3\times10^{-3}$ at a height 1 m above the bed. The use of a constant z_o based on grain roughness neglects effects of a rippled bed, wave-current interaction and near-bed stratification. However, this value is close to the value of $C_D = 1.0\times10^{-3}$ obtained by Feddersen et al. (1998) from a best fit between wind stress and bottom stress seaward of the surf zone at Duck, NC. In addition to the quadratic drag law, a linear drag coefficient of 5×10^{-4} m/s is also tested for consistency with the study of Lentz et al. (1999). Since detailed measurements of the bottom boundary layer are not available to constrain bottom stress estimates in this study, these simple formulations are used for consistency with previous literature, and the implications of uncertainty in the physics will be discussed.

Reliable estimates of the alongshore pressure gradient are not available at either location during the time period of this study. Attempts were made to estimate this term at FRF using tide gauge data, adjusted for barometric pressure, from the mouth of Chesapeake Bay, Duck and Oregon Inlet, NC. However, checking these calculations with pressure data from the CoOP field study (Lentz et al., 1999) showed only weak correlations (not shown). For this reason, the alongshore pressure gradient term is not included in the momentum balance analysis, but its importance will be discussed based on past studies at FRF and MVCO (Lentz et al., 1999; Fewings and Lentz, 2010).

4. Results

a. Description of variability over the inner shelf

Basic descriptions of wind forcing, stratification and velocity are presented first to provide context for the momentum balance analysis. Seasonal variations in wind stress and stratification are compared at FRF and MVCO. Then, a subset of the observations at FRF are presented to illustrate variability at time scales from days to weeks.

Stratification has the potential to influence nonlinear momentum fluxes by promoting the development of cross-shelf exchange and vertical shear. Density stratification, expressed as buoyancy frequency $N = \sqrt{-\frac{g}{\rho_o}\frac{\partial \rho}{\partial z}}$, exhibits a strong seasonal cycle at both the FRF and MVCO sites (Fig. 2a,b). Differences in the monthly means of stratification between the two locations are due in part to methodological differences. At MVCO, monthly means of stratification are estimated from density differences at moored sensors between 1-4.5 m at the 7 m site, and between 1-9.5 m at the 12 m site (Fig. 2b, solid lines). At FRF, stratification is estimated from density differences between 1-7 m from CTD casts conducted during the day, when higher stratification is expected due to the daily cycle of surface heat flux (2b, solid lines). Using the climatology of the daily maximum at the 7 m site at MVCO, in an attempt to account for daytime sampling bias and differences in bottom depth, still indicates that the FRF site is typically more stratified during all times of the year (Fig. 2b, dashed line). Weaker stratification at MVCO may be due to mixing driven by stronger tidal currents. At both locations, highest levels of stratification occur during the months of June-August. The analysis of nonlinear momentum fluxes focuses primarily on these months when strongest stratification is present. However, comparisons of seasonal statistics will be made the months of June–August and periods of weaker stratification during January–March. In addition, moored density time series from throughout the year at MVCO will be used to examine the role of stratification and cross-shelf density gradients.

In addition to stratification, differences in wind forcing between FRF and MVCO also

contribute to differences in physical dynamics (Fig. 2c,d). At FRF, during the months of June-August, wind stress is most commonly oriented offshore (positive τ^{sx}) and upwelling favorable (positive τ^{sy}). At MVCO, wind stress is most commonly oriented with onshore τ^{sx}, but upwelling favorable τ^{sy}. Wind stresses are not strongly polarized in the alongshore direction at either site, unlike many locations on the US west coast where the winds are steered by coastline topography.

The relationship between alongshore wind stress and cross-shelf transport differs between FRF and MVCO during the stratified period of June-August. At FRF, periods of offshore and upwelling favorable wind stress are typically associated with offshore surface layer transport U_s, consistent with upwelling circulation (Fig. 3a). Reversals to onshore and downwelling favorable wind stress at this site are typically associated with onshore U_s. The relationship between wind forcing and cross-shelf transport is more complex at MVCO, where offshore U_s is typically present during a wide range of wind conditions (Fig. 3b). Offshore U_s at this site is observed during onshore and upwelling-favorable wind forcing, as well as reversals to offshore and downwelling favorable conditions. Weak onshore U_s is present some of the time during onshore and downwelling favorable wind stress, and during events in which wind stress is directly onshore with no alongshore component. However, the magnitude of onshore U_s at MVCO is not as high as that observed during similar conditions at FRF. Offshore U_s is present at MVCO during periods of weak wind stress, consistent with the presence of a background mean upwelling circulation that has been previously identified at this site (Fewings et al., 2008; Fewings and Lentz, 2011).

A subset of the FRF time series from 2013 is now used to describe wind forcing and circulation patterns at time scales of days–weeks (Fig. 4). In the next section, it will be shown that these circulation patterns influence the momentum balance through the cross-shelf divergence of nonlinear momentum fluxes. Data from the FRF site are used to present these patterns in time series form due to the relatively clear relationship between cross-shelf transport and wind stress (Fig. 3). During the 45-day time period from 13-

June to 28-July 2013, wind stress typically varies between offshore, upwelling-favorable conditions and onshore, downwelling favorable winds (Fig. 4a). Surface transport U_s typically varies together at the three mooring sites from 5-8 m, increasing with offshore distance (Fig. 4b). The reduction of U_s near the coast is a characteristic pattern of the inner shelf region. Strong vertical shear in the alongshore current, $\partial v/\partial z$, is also present during this time period at both the 6 m and 8 m sites (Fig. 4c). The vertical shear is estimated from differences between 2.0-7.5 m at the 8 m site, and between 2.0-5.0 m depth at the 6 m site. Positive $\partial v/\partial z$ at both sites is generally associated with offshore U_s, as well as offshore and upwelling favorable winds. The combination of vertical shear, cross-shelf exchange and cross-shelf variations in the circulation provide the necessary conditions for nonlinear terms to be potentially important in the alongshore momentum balance.

b. Role of nonlinear terms in depth-averaged momentum balances

The dynamical importance of the nonlinear momentum flux divergence is compared with other terms in the depth-averaged alongshore momentum balance (equation 3). Comparisons of the magnitude and timing of the different terms are first made using the subset of the time series at FRF (Fig. 4), then in a statistical analysis of all available data. The nonlinear term, estimated from the 6 m and 8 m sites at FRF, is positive during much of the 45-day period (Fig. 4d). When wind stress and the nonlinear term are both positive, nonlinear momentum fluxes associated with upwelling circulation play a role in balancing the wind stress. In this case, alongshore momentum is transferred to the ocean by the surface stress, but there is a net offshore flux of alongshore momentum. There are also events (e.g. at 22-June and 26-July) when the wind stress is downwelling-favorable, but the nonlinear term is still positive. In this case, a net onshore flux of negative alongshore momentum during downwelling reinforces negative τ^{sy} on the inner shelf.

The magnitude of the nonlinear term is comparable to other terms in the momentum balance. Although the nonlinear term does not completely balance the wind stress during the period of sustained upwelling-favorable winds from 24-June to 12-July, it is large

enough to make a dynamically important contribution (Fig. 4d). Bottom stress, estimated using the logarithmic layer formulation, is also too small to balance wind stress during this upwelling-favorable period (Fig. 4e). In contrast, the magnitude of the bottom stress is larger than that of the wind stress during the downwelling favorable events at 22-June and 26-July. These patterns are consistent with the contribution of a positive nonlinear momentum flux divergence term during both upwelling and downwelling conditions.

Additional terms also play a role in the alongshore momentum balance. Acceleration is important during certain periods of fluctuating bottom stress, which indicate reversals in the direction of the alongshore flow (Fig. 4e). Estimates of the alongshore pressure gradient are unavailable in this study, but drops in practical salinity below 30 do occur (Fig. 4f), indicating the presence of a buoyant plume originating at the mouth of the Chesapeake Bay (Rennie et al., 1999; Lentz and Largier, 2006). The buoyant plume is associated with southeastward flow and an alongshore pressure gradient force in the negative y direction. The timing of the low-salinity events indicates that the alongshore pressure gradient contributes to negative τ^{by} during periods of weak or upwelling-favorable wind stress, and may also play a role during periods of large bottom stresses that exceed the downwelling-favorable wind stress, in addition to the nonlinear momentum flux divergence.

Since wind stress and bottom stress have previously been identified as the dominant terms in the alongshore momentum balance at FRF (Lentz et al., 1999), the role of the nonlinear term in modifying the balance between these two terms is examined using all of the available data at the 6 m and 8 m sites during June–August. The alongshore wind stress is compared to three response variables: 1) bottom stress only (Fig. 5, BS); 2) the sum of bottom stress and nonlinear momentum flux divergence (Fig. 5, BS+NL); and 3) the sum of bottom stress, nonlinear momentum flux divergence and local acceleration (Fig. 5, BS+NL+A). Similar correlation coefficients of $r = 0.72$-0.77 are obtained for all three response variables, although the correlations are slightly lower when the nonlinear term is included in the response. Using a linear drag coefficient following Lentz et al. (1999)

yields a similar range of correlation coefficients, $r = 0.72$-0.75 (not shown). Despite the similarity of the correlation coefficients obtained with different response variables, examining bin averages of the response by wind stress shows that the nonlinear term does have an impact on the dynamical balance, and that this impact is greater than that of the acceleration term (Fig. 5). Inclusion of the nonlinear terms results in a closer balance with the wind stress. Consistent with the time series variability described above, the magnitude of the response is reduced for downwelling-favorable wind stress and increased for upwelling-favorable wind stress when the nonlinear term is included. These asymmetric changes under different wind conditions are not captured by linear regression analysis and are not improved by tuning bottom drag coefficients.

To examine the role of wind forcing, the dependence of the nonlinear term on wind stress is compared at the FRF and MVCO locations, focusing primarily on the stratified period of June-August. At FRF, the response to wind stress is typically positive regardless of whether τ^{sy} is positive or negative (Fig. 6a), consistent with the time series described above at the same sites on the 6m and 8m isobaths (Figs. 4d, 5). The slopes of the regressions between wind stress and nonlinear terms have the same sign when other pairs of sites are examined; positive slopes are obtained for upwelling favorable wind stress and negative slopes are obtained for downwelling favorable wind stress (Table 1). However, the results obtained for downwelling favorable wind stress are less robust since the regression slopes are significantly different from zero for only three of the five pairs of sites. In addition, the regression slope obtained for the shallowest sites at 5m and 6m during upwelling favorable wind stress is only marginally significant, possibly due to the difficulty in observing small differences in the momentum flux between sites in close proximity. In general, these results from FRF during stratified period of June-August show that the nonlinear term is typically positive regardless of wind direction, but the correlation between the nonlinear term and the alongshore wind stress is more consistent during periods of upwelling favorable wind stress.

At MVCO, there is a different relationship between wind stress and the nonlinear term. The nonlinear term at MVCO is positive for upwelling-favorable wind stress and negative for downwelling-favorable wind stress (Fig. 6b). This different response to downwelling-favorable winds at MVCO compared with FRF is consistent with the differences in surface transport and cross-shelf wind stresses. At MVCO, an offshore surface transport is typically present even when the alongshore component of wind stress is downwelling-favorable (Fig. 3d). The strength and direction of vertical shear in the alongshore current, however, is sensitive to the alongshore wind stress (Fewings et al., 2008). Variability of vertical shear in response to alongshore wind stress and cross-shore density gradients will be examined in greater detail in Section 2.d.

In addition to the patterns in the relationships observed, the magnitude of the nonlinear term relative to the wind stress also differs between locations. The regression slope of 0.15 between the two terms at MVCO during June–August is smaller than those obtained at FRF during upwelling favorable winds ((Fig. 6, Table 1). Comparing the standard deviations of the two terms also shows that the nonlinear term has a greater contribution to the momentum balance at FRF than MVCO (Fig. 7). There are also consistent differences between seasons at each location (Fig. 7). At both locations, the relative importance of the nonlinear term decreases during the months of January–March when the water column is more weakly stratified (Fig. 2).

c. Role of nonlinear terms in surface layer momentum balances

The momentum balance integrated over the surface layer (equation 5) provides a framework for linking nonlinear momentum fluxes to cross-shelf exchange and turbulent stresses. As in the previous section, the roles of the nonlinear terms are compared between FRF and MVCO. The cross-shelf flux divergence is combined with the vertical flux to show the net effect of nonlinear momentum fluxes integrated over the surface layer.

During the stratified months of June–August at FRF and MVCO, the alongshore wind stress term is compared with two different response variables in the momentum balance

of the surface layer: 1) the Coriolis force (fU_s) only and 2) the nonlinear terms. At FRF, the Coriolis force is correlated with the alongshore wind stress during both upwelling-favorable and downwelling-favorable conditions (Fig. 8a). The regression slopes are significantly less than one in each case, indicating that surface transport is significantly reduced from the theoretical Ekman transport $U_{Ek} = \tau^{sy}/\rho_o f$ expected in deeper water. At MVCO, the regression slope between the Coriolis force and wind stress during upwelling-favorable conditions is smaller than at FRF (Fig. 8c). During downwelling-favorable wind stress at MVCO, the regression slope is only marginally statistically significant but negative (Fig. 8c). This pattern is consistent with the consistent offshore transport that occurs at this location, even during downwelling favorable wind stress (Fig. 3b).

At both locations, inclusion of the nonlinear terms impacts the alongshore momentum balance of the surface layer. At FRF, similar to the depth-averaged momentum balance shown in Section 4.b, the relationship between the wind stress and the nonlinear terms changes depending on the direction of the alongshore wind stress (Fig. 8b). During upwelling-favorable winds at FRF, the positive regression slope between the wind stress and the nonlinear terms (0.35 ± 0.15) indicates that a substantial fraction of the momentum put into the ocean by wind stress is transferred offshore by the nonlinear momentum fluxes associated with the upwelling circulation, in addition to being transferred downward by the turbulent stress at the base of the surface layer (Fig. 8a). Based on the regression coefficient, the impact of nonlinear momentum fluxes exceeds that of the Coriolis force. Under downwelling favorable conditions at FRF, the regression slope is only marginally different from zero (Fig. 8b). In this case, positive values of the nonlinear term are consistent with a transfer of momentum from offshore by the nonlinear momentum fluxes associated with the downwelling circulation, as well as an enhanced interior stress whose magnitude exceeds that of the wind stress.

The nonlinear terms have a less significant impact on momentum balance of the surface layer at MVCO, and once again there are differences from the dynamics observed at

FRF. At MVCO, the nonlinear terms tend to be positive during upwelling favorable winds and negative during downwelling favorable winds (Fig. 8d). The regression slope is significant, but the correlation of r^2 = 0.27 indicates substantial scatter in the relationship. A piece-wise linear fit is only significant for the negative values of τ^{sy}. However, the overall trend is consistent with the depth averaged balance at the same site (Fig. 6b). Unlike FRF, the nonlinear momentum fluxes at MVCO tend to balance the alongshore wind stress during both upwelling-favorable and downwelling-favorable conditions. The presence of persistent offshore surface transport at MVCO, even when the alongshore component of wind stress is downwelling-favorable, alters the relationship between the nonlinear terms and alongshore wind stress at this site. The influence of cross-shelf wind stress on surface transport likely contributes to the variability of the nonlinear term, which depends in part on the strength of cross-shore circulation.

d. Role of density structure and processes influencing vertical shear

Time series of density from moorings at MVCO provide the opportunity to examine the influence of the density structure on the nonlinear dynamics of the alongshore momentum balance. Density stratification and cross-shelf density gradients can influence nonlinear momentum fluxes through their roles in governing mixing, cross-shelf exchange and vertical shear. This section specifically focuses on the processes governing vertical shear in the alongshore flow, which must be present for the nonlinear term to contribute to the alongshore momentum balance. There are several potential mechanisms for the generation of vertical shear, including thermal wind balance and frictional stresses. Hypothetical predictions of vertical shear involving the cross-shelf density gradient and surface wind stress are now examined under different levels of stratification.

The hypothetical predictions are evaluated at the 7 m and 12 m sites at MVCO. The analysis focuses on depths where density and velocity data are available at both of these sites. Vertical shear is computed from velocity differences between 3 m and 5 m depths. The horizontal density gradient is computed from averages of density observations at

depths of 3 m and 5 m at each site. Results are categorized based on the buoyancy frequency N, calculated from averages of the 7 m and 12 m sites. A value of $N = 0.01$ s^{-1} is chosen to characterize periods of relatively weak and strong stratification. Based on climatological averages (Fig. 2b), periods of $N < 0.01$ s^{-1} are typical during October–March while stronger stratification is present during April–September.

i. Geostrophic shear and thermal wind balance If the cross-shelf momentum balance is geostrophic, the vertical shear is proportional to the cross-shelf density gradient and determined by thermal wind balance

$$\frac{\partial v}{\partial z} = -\frac{g}{f\rho_o}\frac{\partial \rho}{\partial x}. \tag{7}$$

At MVCO, the cross-shelf density gradient $\partial\rho/\partial x$ is typically positive (density increases offshore), which is consistent with negative $\partial v/\partial z$ in a hypothetical thermal wind balance (Fig. 9a). Although upwelling circulation is often associated with negative $\partial\rho/\partial x$ at other locations, a combination of surface heating and vertical mixing maintain a positive density gradient at MVCO (Fewings and Lentz, 2011). During periods of weak stratification, $\partial\rho/\partial x$ is relatively small and sometimes negative. The two terms in the thermal wind balance are weakly correlated during both strongly stratified periods (r = 0.44, $p < 0.001$, slope = 0.55) and weakly stratified periods (r = 0.51, p = 0.03, slope = 0.37). However, there are times when there is clear disagreement. In particular, thermal wind balance fails to explain positive values of $\partial v/\partial z$. It should be noted that comparing the terms of the thermal wind balance is challenging using measurements from two moorings. The estimates of vertical shear at the 7m and 12m sites are only weakly correlated with each other (r = 0.53 during stratified periods, r = 0.55 during unstratified periods) and small-scale density fronts may be unresolved. The agreement with thermal wind balance is not improved when the vertical shear from individual sites are used in place of the average, except when the 7m site is used during unstratified periods (increasing r slightly from

0.51 to 0.55). Although unresolved gradients may be a factor, estimates from the available measurements suggest that there is substantial ageostrophic shear which is associated with deviations from thermal wind balance.

ii. Wind-supported shear In addition to geostrophic processes, which are inviscid and depend on the Earth's rotation, vertical shear can also be associated with the presence of turbulent stresses in the water column. To test whether the magnitude of the observed vertical shear $\partial v/\partial z$ is consistent with generation of frictional stresses by the wind, a hypothetical relationship based on a simple form of the eddy viscosity A is considered. Eddy viscosity over the inner shelf is expected to vary as a function of stratification, surface buoyancy fluxes, advection of the density field and distance from the boundaries. Although the data used in this study cannot resolve the complexity of turbulent stresses over the inner shelf, a simplified form of the eddy viscosity is used to compare the strength of hypothetical wind-supported shear relative to the geostrophic shear. In modeling a river plume under downwelling-favorable wind stress, Chen and Chen (2017) found the vertical shear to be consistent with the relationship

$$\frac{\partial v}{\partial z} = \frac{\tau^{sy}}{\rho_o A}, \tag{8}$$

where $A = \kappa u_* h/6$, and $u_* = \sqrt{|\tau^{\mathbf{s}}|/\rho_o}$ is a friction velocity based on the magnitude of the surface stress $|\tau^{\mathbf{s}}|$. This provides an estimate of the depth-averaged shear when the alongshore stress $A\partial v/\partial z$ is constant throughout the water column and determined completely by the wind stress. The choice of constant A is consistent with the depth-average of a parabolic vertical profile of A (Chen and Chen, 2017). The hypothetical wind-supported shear in equation (8) is expected to be most relevant when the water column is unstratified.

Like the geostrophic shear, the hypothetical wind-supported shear alone cannot completely explain the observations (Fig. 9b). There is a significant correlation during periods

of weak stratification (r = 0.74, $p < 0.001$, slope = 0.40), but the expression for wind-supported shear in equation (8) does not account for the presence of negative $\partial v/\partial z$ during weak wind stress and the regression slope suggests that this relationship underestimates the observed vertical shear. During stratified periods, the terms are also correlated (r = 0.71, $p < 0.001$, slope = 1.41) but there are large discrepancies between the magnitudes of the observed shear and theoretical predictions. Some of the negative $\partial v/\partial z$ values that are inconsistent with the magnitude of the wind-supported shear can be explained by thermal wind shear (Fig. 9a). Positive values of $\partial v/\partial z$ that cannot be explained by thermal wind balance during periods relatively strong stratification occur during periods of positive τ^{sy} and strong wind-supported shear (9b). It is therefore likely that the observed vertical shear results from the combined effects of geostrophic and frictional processes.

iii. Combined geostrophic and wind-supported shear Cross-shelf density gradients and wind stress both likely play a role in determining the strength and direction of the vertical shear, and therefore the nonlinear fluxes of alongshore momentum. Stratification also likely plays an important role in modulating vertical shear. Although thermal wind balance does not completely explain the vertical shear at MVCO, the residual is significantly correlated with the alongshore wind stress during stratified periods (Fig. 10a, r = 0.62, p < 0.001). Over the same range of alongshore wind stress values, variations in vertical shear and the thermal wind balance residual are significantly reduced during unstratified periods when cross-shelf density gradients are also relatively small (Figs. 9, 10a). These results suggest that the wind stress can be effective at generating ageostrophic shear over the inner shelf when the water column is stratified.

The presence of vertical shear is essential for the nonlinear term to have a role in the depth-averaged alongshore momentum balance. The relationship between alongshore wind stress and vertical shear, combined with upwelling circulation, leads to a weak but significant correlation between along-shelf wind stress and the nonlinear term at MVCO when the water column is stratified (Fig. 10b, r = 0.44, $p < 0.001$, slope = 0.18). During

weakly stratified time periods, the magnitude of the nonlinear term is much smaller over a similar range of τ^{sy} values. Although the relationship between alongshore wind stress and the nonlinear term differs between locations (Fig. 6), vertical shear is expected to vary in response to thermal wind balance and alongshore wind stress at all inner shelf locations.

5. Discussion

a. Circulation patterns associated with nonlinear momentum fluxes

To summarize circulation patterns associated with nonlinear momentum fluxes over the inner shelf, conceptual models are presented based on results from this study and previous studies at the same locations (Fig. 11). Focusing on the strongly stratified season during June–August, differences are highlighted between the North Carolina inner shelf at FRF and the New England inner shelf at MVCO. At each of these locations, circulation patterns and dynamics are compared between different wind forcing conditions. Differences in surface heat flux, tidal mixing and larger-scale circulation also contribute to differences in the vertical and cross-shelf structure of the density field at these two locations.

i. North Carolina inner shelf Flow patterns and dynamics associated with upwelling circulation over the inner shelf are first described based on observations at the FRF site (Fig. 11a). The most common wind pattern at FRF in North Carolina is upwelling favorable and offshore (Fig. 2c). This type of wind forcing is strongest before the passage of an atmospheric cold front and is also associated with the strongest surface heat fluxes from the atmosphere to the ocean (Austin and Lentz, 1999). Not surprisingly, upwelling favorable and offshore wind forcing is typically associated with offshore transport in the surface layer (Fig. 3a). As observed by Lentz (2001), the magnitude of U_s increases with water depth but typically remains less than the theoretical deep water Ekman transport U_{Ek} at sites where water depth $h < 10$ m (Fig. 4b, 8a). The positive divergence of cross-shelf surface transport $\partial U_s/\partial x$ is consistent with upward vertical velocity w_L over

the inner shelf. Hydrographic observations offshore of FRF during upwelling-favorable wind forcing in August show a shoaling of the thermocline near shore (Austin and Lentz, 1999; 2002; Cudaback and Largier, 2001), which is also consistent with the presence of an upwelling circulation.

Upwelling-favorable and offshore wind forcing at FRF is also often associated with strong positive vertical shear $\partial v/\partial z$ (Fig. 11a). The vertical shear reaches similar values at different mooring sites at FRF (Fig. 4c). The positive sign of $\partial v/\partial z$ is consistent with thermal wind balance associated with negative $\partial \rho/\partial x$ as the thermocline shoals and cold, dense water is upwelled near the coast. Density time series for estimating $\partial \rho/\partial x$ are not available during the time period analyzed in this study, but previous observations show significant correlations between the two terms in the thermal wind balance (Lentz et al., 1999). However, Lentz et al. (1999) found weaker agreement with thermal wind balance at the shallowest sites (8–13 m), and the largest disagreements appear to be during times when $\partial v/\partial z$ is positive. In addition to geostrophic thermal wind shear, it is therefore likely that wind forcing contributes directly to vertical shear by generating turbulent stresses.

The circulation patterns established during upwelling-favorable and offshore wind stress at FRF (Fig. 11a) lead to a divergence of the cross-shelf flux of alongshore momentum, a nonlinear process that influences the alongshore momentum balance. The combination of offshore U_s and positive $\partial v/\partial z$ creates a net offshore flux of positive alongshore momentum when integrated over the water column, $\int_{-h}^{\eta} (u_L v)\, dz$, since the onshore return flow in the lower layer is associated with relatively small v compared with the surface layer. This flux increases with offshore distance as offshore transport increases and as the surface-to-bottom velocity difference increases for similar $\partial v/\partial z$. This mechanism is similar to that described by Lentz and Chapman (2004) for upwelling conditions at mid-shelf locations. However, the dynamics are modified over the inner shelf because U_s changes with offshore distance and there is no clear separation between the surface and bottom boundary layers.

During downwelling-favorable and onshore wind forcing, the circulation patterns are essentially reversed over the inner shelf at FRF (Fig. 11b). This type of wind forcing is commonly associated with the passage of atmospheric cold fronts (Austin and Lentz, 1999). During these conditions, surface-layer transport typically reverses to onshore (Fig. 3a). The onshore surface layer transport U_s is reduced from U_{Ek}, and there is a convergence $\partial U_s/\partial x < 0$ consistent with downward w_L (Lentz, 2001). Hydrographic data indicate the presence of a downwelling front, with water of uniform temperature onshore of the front (Austin, 1999; Cudaback and Largier, 2001). The cross-shelf circulation associated with downwelling over the inner shelf is time-dependent, and has been shown in some cases to shut down after the downwelled isotherms move offshore (Lentz, 2001). However, the time-dependent density structure can be complicated by the arrival of salinity associated with the Chesapeake Bay freshwater plume, which lags negative (downwelling-favorable) τ^{sy} (Cudaback and Largier, 2001). During weak or moderate downwelling-favorable wind stress, the plume can promote stratification onshore of the downwelled isotherms and create a region of positive $\partial\rho/\partial x$ and negative $\partial v/\partial z$ (Cudaback and Largier, 2001), which is qualitatively consistent with thermal wind balance. The vertical shear in the alongshore flow is enhanced during periods of downwelling-favorable wind stress, which promotes mixing of the plume during periods of relatively strong downwelling-favorable wind stress (Lentz and Largier, 2006). The presence of mixing in the plume during both upwelling-favorable and downwelling-favorable wind stress leads to ageostrophic shear and deviations from thermal wind balance (Mazzini et al., 2019).

The circulation patterns associated with downwelling winds at FRF (Fig. 11b) lead to a positive momentum flux divergence. This nonlinear term in the depth-averaged momentum balance has the same positive sign during both upwelling and downwelling (Fig. 6a). This is generally consistent with the idealized modeling study of Kuebel Cervantes et al. (2004), in which the nonlinear terms make a mean positive contribution inshore of

an upwelling front under periodic wind forcing. A similar pattern of positive momentum flux divergence during both upwelling-favorable and downwelling-favorable wind stress is also present when the fluxes are integrated over the surface layer (Fig. 8b), consistent with a net onshore flux of negative momentum in the surface layer. Time dependence of the cross-shelf circulation, and the presence of a freshwater plume, likely contribute to variability of this term during downwelling-favorable winds.

ii. New England inner shelf At MVCO, the relationship between wind forcing and nonlinear momentum flux divergence is less straightforward. During the stratified season of June–August, winds are often either upwelling-favorable and onshore, or downwelling-favorable and offshore (Fig. 2d). The wind stress components τ^{sy} and τ^{sx} therefore often oppose each other in their contributions to U_s. Offshore U_s is commonly observed during a wide range of wind forcing conditions, including weak wind stress, consistent with persistent upwelling circulation throughout the stratified season (Fig. 3b). However, the density structure differs from that observed at FRF. Warmer, lighter water is typically present near shore, consistent with observations of positive $\partial\rho/\partial x$ (Fig. 9a). Fewings and Lentz (2011) show that the presence of warmer and lighter water near shore is consistent with a combination of surface heat flux warming shallow waters and strong vertical mixing. Compared with the North Carolina shelf, the New England shelf is characterized by stronger tides, facilitating strong vertical mixing.

In the alongshore component of velocity, mean negative (westward) $\bar{v}$ is present, likely due to a combination of a large-scale mean alongshore pressure gradient (Lentz, 2008b; Xu and Oey, 2011) and tidal rectification near shoals to the east of the mooring array (Ganju et al., 2011; Kirincich et al., 2013). However, conditional averages of velocity during alongshore wind forcing in winter months show that positive τ^{sy} in the range 0.5–1.0 Pa is sufficient to reverse the alongshore flow to positive v, and create positive $\partial v/\partial z$ (Fewings et al., 2008). Conditional averages of velocity at MVCO during combined τ^{sy} and τ^{sx} forcing and weak stratification show v in the same direction as the alongshore

component of wind stress (Kirincich, 2013). This pattern is consistent with model results which show that alongshore wind stress is more effective than cross-shelf wind stress at driving alongshore velocity (Tilburg, 2003). Reversals in alongshore velocity can occur without a corresponding reversal in U_s at this location. However, prior studies that have examined the vertical structure of alongshore currents under different wind conditions at MVCO have primarily focused on periods of weak stratification.

In the stratified season at MVCO, during upwelling-favorable and onshore wind forcing, circulation patterns are often characterized by offshore U_s and positive $\partial v/\partial z$ (Fig. 11c). These patterns are similar to those observed during upwelling-favorable wind forcing at FRF (Fig. 11a), except for the positive cross-shelf density gradient $\partial \rho/\partial x$. As a result, positive τ^{sy} is generally associated with positive momentum flux divergence in both the depth-averaged and surface-integrated momentum balances (Figs. 6b, 8d). The presence of positive $\partial v/\partial z$ is inconsistent with thermal wind balance and positive $\partial \rho/\partial x$ (Fig. 9a, Section 2.d.i). However, the presence of positive $\partial v/\partial z$ can be explained by ageostrophic shear generated by the wind stress (Figs. 9b, 10). Deviations from thermal wind balance are likely to occur over the inner shelf, where turbulent stresses occur throughout the water column, which suggests that the theory developed for mid-shelf locations by Lentz and Chapman (2004) does not fully explain the dynamics over the inner shelf.

During downwelling-favorable and offshore wind forcing at MVCO, circulation patterns are characterized by offshore U_s and negative $\partial v/\partial z$ (Fig. 11d). The presence of negative $\partial v/\partial z$ can be attributed to a combination of thermal wind balance and wind-induced shear (Figs. 9, 10a). The presence of upwelling circulation and negative $\partial v/\partial z$ leads to negative momentum flux divergence during negative τ^{sy} in both the depth-averaged and surface-integrated momentum balances (Figs. 6b, 8d). During downwelling favorable winds at MVCO, this nonlinear term tends to balance negative τ^{sy} due to a net offshore flux of negative momentum. This differs dramatically from downwelling-favorable condi-

tions at FRF, where a net onshore flux of negative momentum tends to reinforce the wind stress. These results show that the contribution of the nonlinear momentum flux divergence depends on the background circulation and cross-shelf component of wind stress, in addition to the along-shelf wind stress.

b. Dynamical importance of nonlinear momentum fluxes

The results of this study indicate that cross-shelf fluxes of alongshore momentum can make a dynamically significant contribution to alongshore momentum balances over the inner shelf. During upwelling-favorable wind forcing over the North Carolina inner shelf, the nonlinear term is significantly correlated with the wind stress term, with a regression slope of 0.57 $\pm$ 0.22 (Fig. 6a, Table 1). During downwelling-favorable wind stress, the sign of the relationship changes, consistent with the circulation patterns described above in Section 5.a. The regression slope of -0.77 $\pm$ 0.51 is statistically significant, but the broad 95% confidence intervals indicate substantial deviations from a linear relationship (Fig. 6a). At MVCO, the nonlinear term tends to partially balance the wind stress with a regression slope of 0.15 $\pm$ 0.03 overall (Fig. 6b). Similar relationships are present in the surface-integrated momentum balance, with smaller regression slopes (Fig. 8b,d).

The observed relationships between the nonlinear terms and wind stress at FRF are qualitatively consistent with the two-dimensional modeling study of Kuebel Cervantes et al. (2003), which includes realistic wind forcing and surface fluxes during the time period of the 1994 CoOP program. During upwelling favorable wind conditions in this model study, the regression slopes between the nonlinear and wind stress terms in the depth-averaged momentum balance are 0.26 at 4 m and 0.33 at 8 m. These regression slopes are smaller than the value of 0.57 found in this study, but still account for an important component of the momentum balance. During downwelling-favorable conditions, the slopes obtained by Kuebel Cervantes et al. (2003) are negative, but with values of -0.037 to -0.035, which are much smaller in magnitude than found here from the observations. Similar to the observational estimates in this study (Fig. 5), the modeled momentum balance

shows different relationships between surface stress and bottom stress depending on the sign of the alongshore wind stress. Neither this study nor the model study of Kuebel Cervantes et al. (2003) account for the alongshore pressure gradient term in the momentum balance, which Lentz et al. (1999) found to improve closure of the momentum balance in the 1994 CoOP observations, although it was uncorrelated with the alongshore wind stress. In addition to influencing the alongshore pressure gradient, the Chesapeake plume also influences the FRF site by promoting density stratification and thermal wind shear (Rennie et al., 1999; Cudaback and Largier, 2001). The presence of salinity stratification likely increases cross-shelf exchange and alters the position of the downwelling front, which may account for some of the differences between this study and the model study of Kuebel Cervantes et al. (2003).

At MVCO, the nonlinear terms play a relatively minor role in balancing the alongshore wind stress. In a previous study of the alongshore momentum balance at this site, which does not include estimates of the nonlinear terms, Fewings and Lentz (2010) demonstrated a dominant balance between the wind stress and the alongshore pressure gradient, with bottom stress making a secondary contribution. Observations of the alongshore pressure gradient are not available during the time period of the SWWIM observations used in this study. However, the regression slope of 0.15 between the wind stress and the nonlinear term found in this study is significantly smaller than the regression slope of 0.9 between the wind stress and alongshore pressure gradient found by Fewings and Lentz (2010). Although it is clearly not the dominant mechanism for balancing the wind stress at MVCO, this contribution of the nonlinear term is likely greatest during periods of strong stratification, when cross-shelf exchange and vertical shear are strongest.

It is possible to estimate the nonlinear term based on a single mooring, rather than a pair of moorings, since there can be no flux of momentum at the coastal boundary. This type of estimate has been used to justify neglecting the nonlinear term in previous studies of the alongshore momentum balance at MVCO (Fewings and Lentz, 2010; Kirincich,

2013). If the vertically integrated momentum flux decreases linearly to the coast at $x = 0$, the momentum flux divergence can be approximated as

$$\frac{\partial}{\partial x}\int_{-h}^{0}(u_L v)\ dz \approx \frac{1}{x}\int_{-h}^{0}(u_L v)\ dz. \tag{9}$$

The approximation in equation (9) was used by Lentz and Chapman (2004) to estimate the momentum flux divergence from single moorings at mid-shelf sites. Over the inner shelf, the observed variability of the depth-integrated momentum flux is consistent with a monotonic decrease towards the coast (Fig. 12). Standard deviations of the depth-integrated momentum flux during June–August are smaller at shallower water depths at both FRF and MVCO. The standard deviations are larger at FRF than MVCO at similar water depths, consistent with a greater importance of the momentum flux divergence term over the North Carolina inner shelf.

To test the validity of the approximation in equation (9), the estimates made from pairs of moorings are compared with the approximation estimated from the deeper moor-ing only (Fig. 13a). The approximation is strongly correlated with the estimates made from the pairs of moorings at FRF ($r = 0.92$) and MVCO ($r = 0.95$) during the stratified months of June–August. However, the approximation in equation (9) underestimates the magnitude of the nonlinear term estimated from pairs of moorings, as indicated by regres-sion slopes of 2.1 at FRF and 1.5 at MVCO. This suggests that the assumption of a linear decrease of the vertically integrated momentum flux near the coast may not be valid. This is confirmed by comparing the standard deviation of the depth-integrated momentum flux at different sites (Fig. 12). The variability is consistent with a quadratic increase with water depth, from zero at the coast, which would result in an underestimate if a linear increase is assumed. The approximation in equation (9) can be used to obtain an order of magnitude estimate of the nonlinear term, and to examine how the nonlinear term varies in time with the wind stress or other forcing, but it may represent a lower bound on the value over the inner shelf.

c. *Factors governing importance of nonlinear momentum fluxes*

The dynamical impact of the nonlinear term is potentially significant, but this impact varies both in time and between different inner shelf locations. To assess the factors that govern the overall importance of nonlinear momentum fluxes, a scaling is developed based on the bottom slope, surface transport and vertical shear. The expected role of the nonlinear term in the physical dynamics of the inner shelf is then discussed based on these commonly observed parameters.

The scaling analysis assumes linear vertical profiles of u_L and v,

$$u_L(z) = \frac{4U_s}{h}\left(1 + \frac{2z}{h}\right), \tag{10}$$

$$v(z) = v_s + \frac{\partial v}{\partial z} z, \tag{11}$$

where v_s is the surface velocity at $z = 0$. The linear cross-shelf velocity profile in equation (10) describes a two-layer flow that satisfies two-dimensional mass balance, $\bar{u}_L = 0$. With the vertical structure of the velocity given by equations (10) and (11), the vertically-integrated cross-shelf flux of alongshore momentum is

$$\int_{-h}^{0} (u_L v)\ dz = \frac{2}{3} U_s \frac{\partial v}{\partial z} h. \tag{12}$$

Two further simplifications are made about the cross-shelf structure of the circulation. First, the ratio of the surface transport U_s to the theoretical Ekman transport U_{Ek} is proportional to the ratio of the water depth h to the boundary layer depth δ_s, so that $U_s \propto U_{Ek} h/\delta_s$ (Lentz and Fewings, 2012). If the vertical shear $\partial v/\partial z$ and boundary layer depth δ_s are independent of h, the depth-integrated flux then depends on h^2, consistent with the observed variability (Fig. 12). Second, a constant bottom slope is assumed so that $h = \alpha x$. With a constant bottom slope α, the surface transport increases with cross-shelf distance $U_s \sim U_{Ek} \alpha x/\delta_s$. With these simplifications, the vertically integrated momentum flux in

equation (12) is proportional to x^2, not x as assumed in the approximation in equation (9). Using these assumptions of the cross-shelf structure, the divergence of the nonlinear momentum flux is

$$\frac{\partial}{\partial x}\int_{-h}^{0}(u_L v)\ dz = \frac{4}{3}\alpha U_s \frac{\partial v}{\partial z}. \tag{13}$$

This scaling highlights the three main factors that influence the magnitude and direction of the momentum flux divergence: 1) the cross-shelf transport U_s, 2) the vertical shear $\partial v/\partial z$, and 3) the bottom slope α. Note that the expression for the divergence of the nonlinear momentum flux in equation (13) does not change if the surface transport is driven primarily by the cross shelf component of the wind stress so that $U_s \propto -V_{Ek}h/\delta_s$, where $V_{Ek} = -\tau^{sx}/\rho_o f$ (Lentz and Fewings, 2012). In both cases, the surface transport increases linearly with water depth h in this simplified scenario. If the alongshore flow is in geostrophic balance, the vertical shear $\partial v/\partial z$ is related to the cross-shelf density gradient through thermal wind balance, as in equation (7). However, the presence of turbulent stresses can introduce ageostrophic shear. Ageostrophic shear contributes significantly to the total vertical shear in wind forced river plumes (Chen and Chen, 2017; Mazzini et al., 2019). Estimates of the ageostrophic shear at MVCO in this study are correlated with the alongshore wind stress at MVCO during stratified conditions (Fig. 10a). It is therefore possible that a turbulent thermal wind balance, in which geostrophic shear is modified by turbulent stresses, often applies over the inner shelf where the water depth and boundary layer thickness are comparable.

To test whether the scaling in equation (12) summarizes the key dynamics of momentum flux divergence over the inner shelf, estimates of the right-hand side are compared with the momentum flux divergence diagnosed from pairs of moorings at FRF and MVCO (Fig. 13b). Estimates of U_s and $\partial v/\partial z$ are obtained from the deeper mooring site in each pair, while the bottom slope between the mooring pair at each location is used for α. The scaling is significantly correlated with the nonlinear term, but underestimates the magni-

tude at both FRF (r = 0.72, p $<$ 0.001, slope = 0.72) and MVCO (r = 0.58, p $<$ 0.001, slope = 0.44). The scaling is consistent with the much greater range in magnitude of the nonlinear term at the FRF site compared with MVCO. Despite the highly simplified vertical and cross-shelf structure on which it is based, the simple scaling agrees reasonably well with the more detailed observational estimates, and can therefore be used to discuss how different aspects of inner shelf circulation and site characteristics influence the role of nonlinear processes.

To compare the importance of the nonlinear term at different inner shelf locations, it is useful to relate its magnitude to the wind stress. The dynamical role of the nonlinear term in the momentum balance can be summarized as a fraction of the alongshore wind stress term,

$$\frac{\frac{\partial}{\partial x}\int_{-h}^{0}(u_L v)\ dz}{\left(\frac{\tau^{sy}}{\rho_o}\right)} = \frac{4}{3}\frac{\alpha}{f}\frac{U_s}{U_{Ek}}\frac{\partial v}{\partial z}. \tag{14}$$

The fraction of theoretical Ekman transport in the surface layer, U_s/U_{Ek}, becomes part of this non-dimensional number. Close to the coast, the fraction of theoretical Ekman transport approaches zero. In the absence of an alongshore pressure gradient, the wind stress is rapidly balanced by bottom friction in these shallow depths. At the boundary of the inner shelf and mid shelf, where U_s/U_{Ek} approaches $\sim$1, the role of the nonlinear term is governed by α, f and $\partial v/\partial z$.

At the boundary of the inner shelf and mid shelf, the relationship between the nonlinear term and the wind stress shares similarities with the theory developed by Lentz and Chapman (2004). This theory is based on assumptions that 1) the surface transport is equal to the theoretical Ekman transport, 2) thermal wind balance is valid, and 3) there is a relationship between the cross-shelf density gradient $\partial\rho/\partial x$ and the stratification $\partial\rho/\partial z$ associated with isopycnals shoaling upward towards the coast. With these assumptions, the role of the nonlinear term in equation (14) could be summarized by the slope Burger

number $S = N\alpha/f$ as in Lentz and Chapman (2004). Although the theory of Lentz and Chapman (2004) is based on a three-layer cross-shelf circulation structure, the presence of an inviscid interior between the surface and bottom boundary layers is not necessary for the nonlinear term to be important. However, a theory based on S may not be appropriate for inner shelf locations, which differ in important ways from the mid-shelf locations in eastern boundary upwelling systems examined by Lentz and Chapman (2004). At MVCO, there is positive cross-shelf density gradient $\partial\rho/\partial x$ and isopycnals slope downward toward the coast even during periods of upwelling-favorable τ^{sy}, which is inconsistent with the upward-sloping isopycnals assumed by Lentz and Chapman (2004). Kirincich and Barth (2009b) found that the importance of the nonlinear term in balancing the wind stress varied at different inner-shelf sites along the same isobath, due to differences in $\partial v/\partial z$ at sites with similar stratification. In addition, compared with mid-shelf sites, thermal wind balance is less well established over the inner shelf. Hydrographic sections and mooring time series do show consistency with thermal wind balance in shallow water (Lentz et al., 1999; Garvine, 2004; Kirincich and Barth, 2009a), indicating that it should play a strong role in determining the vertical shear. At MVCO, thermal wind balance partially explains variability in $\partial v/\partial z$, but does not account for positive $\partial v/\partial z$ during upwelling-favorable wind stress (Section 4.d). Thermal wind balance may be more important at FRF where stratification is stronger and $\partial v/\partial z$ varies over a wider range, although Lentz et al. (1999) found this relationship to be weakest in shallow water.

Comparing the FRF and MVCO locations based on the three key factors of bottom slope, surface transport and vertical shear helps explain differences in the magnitude and relative importance of the nonlinear terms at each site. The regression slope between the nonlinear term and the wind stress is 0.57 at FRF during upwelling-favorable wind stress, and 0.15 at MVCO over all wind forcing conditions (Fig. 6). Differences in bottom slope between the two locations, $\alpha = 6.4 \times 10^{-3}$ at FRF and $\alpha = 4.5 \times 10^{-3}$ at MVCO, are relatively minor. For context, both of these values are in the middle of the range

of bottom slopes at the mid-shelf sites examined by Lentz and Chapman (2004), which range from 1.5×10^{-3} to 10^{-2}. Although the continental shelf is relatively broad in the Mid-Atlantic Bight, both mooring arrays examined in this study are located over steeper nearshore bathymetry. Differences in f of 8.6×10^{-5} s^{-1} at FRF and 9.6×10^{-5} s^{-1} at MVCO are also relatively minor. However, vertical shear and cross-shelf transport both differ substantially between the FRF and MVCO locations. Values of $\partial v/\partial z$ vary between -2.1 $\times$ 10^{-2} and 1.2 $\times$ 10^{-2} s^{-1} at MVCO (Fig. 9) but vary over a much larger range from -7.0 $\times$ 10^{-2} to 7.0 $\times$ 10^{-2} s^{-1} at FRF (Fig. 4c). Based on regression slopes between fU_s and τ^{sy}/ρ_0 during upwelling-favorable wind stress, the fraction of Ekman transport U_s/U_{Ek} is 0.20 $\pm$ 0.08 at the 6–8m sites examined at FRF, and a much lower fraction 0.06 $\pm$ 0.03 at the 7–12m sites examined at MVCO despite their greater average depth (Fig. 8a,c). Differences in the role of the nonlinear terms at FRF and MVCO are best explained by a combination of the strength of the cross-shelf circulation and the vertical shear in the alongshore flow. The lower fraction of Ekman transport and the reduced vertical shear at MVCO may be a result of stronger vertical mixing associated with stronger tidal currents over the New England inner shelf.

The bottom slope can be an important parameter because it helps determine the cross-shelf scale of the momentum flux divergence. For example, the nonlinear momentum flux divergence has been found to play a major role in balancing the wind stress at sites onshore of Heceta Bank over the Oregon inner shelf (Kirincich and Barth, 2009b). This region has a relatively steep slope of α =0.0125, steeper than the two locations examined in this study. Vertical shear estimated from a shipboard survey at this site gives $\partial v/\partial z \approx$ 1 $\times$ 10^{-2} s^{-1} (Kirincich and Barth, 2009a), which is similar to the magnitude observed at MVCO (Fig. 10). At the 15m isobath off Oregon, where $U_s/U_{Ek} \approx 0.4$ (Kirincich et al., 2005), equation (14) gives an estimate of $\sim$0.67 for the ratio of the nonlinear and wind stress terms. In contrast to this large influence of the nonlinear term over a steeply sloping inner shelf, the influence of the nonlinear term is expected to be much smaller at

inner shelf locations with similar vertical shear but smaller bottom slopes. Over the west Florida inner shelf, $\partial v/\partial z$ can reach values of $\sim 2 \times 10^{-2}$ s^{-1} (Weisberg et al., 2001), but the bottom slope of $\alpha \approx 8 \times 10^{-4}$ is relatively small. In this case, equation (14) gives an upper bound of $\sim$0.33 for the ratio of the nonlinear and wind stress terms at the boundary of the inner shelf and mid-shelf, consistent with a relatively minor role of the nonlinear terms in modeled alongshore momentum balances (Li and Weisberg, 1999; Weisberg et al., 2001). Similarly, the nonlinear momentum flux divergence is also expected to play a minor role over the New Jersey inner shelf, where $\alpha \approx 10^{-3}$ and $\partial v/\partial z$ reaches values of $\sim 1 \times 10^{-2}$ (Garvine, 2004). Although a moderate value of $S \approx 0.7$ over the New Jersey inner shelf suggests that nonlinear terms should be important based on the theory of Lentz and Chapman (2004), equation (14) gives an upper bound of $\sim$0.14 for the ratio of the nonlinear and wind stress terms at the boundary of the inner shelf and mid-shelf. Although Garvine (2004) did not estimate the magnitude of the nonlinear term, bottom stress was found to be substantial relative to the wind stress. Although the bottom slope plays an important role in determining the importance of nonlinear momentum fluxes over the inner shelf, dependence on the slope Burger number S may not be always applicable in the same manner as mid-shelf sites in coastal upwelling regions.

The dynamical role of nonlinear momentum flux divergence is determined by a complex set of interactions between stratification, turbulent mixing, cross-shelf exchange and the alongshore flow, all of which are influenced by wind forcing. The nonlinear term reaches greater magnitudes when stratification values of $N > 0.01$ s^{-1} are present at MVCO (Fig. 10b). Stratification promotes cross-shelf exchange by reducing the boundary layer thickness and the turbulent stress at the base of the surface layer. Stratification can also promote the development of vertical shear by inhibiting shear instability. In addition to vertical density stratification, the cross-shelf density gradient has also been shown to influence mixing and exchange when the inner shelf is forced by cross-shelf wind stress (Horwitz and Lentz, 2014). The cross-shelf density gradient also influences vertical shear

of the alongshore flow through thermal wind balance. Cross-shelf fluxes of alongshore momentum are therefore coupled with the cross-shelf advection of density. Cross-shelf fluxes of alongshore momentum can also influence mixing by reducing the role of bottom friction on the inner shelf, which can then promote near-bottom stratification in a positive feedback mechanism.

A limitation of this study is that that it does not account for the effects of three dimensional circulation over the inner shelf. Although the two long-term mooring arrays at FRF and MVCO allow for calculation of the cross-shelf divergence of the momentum flux, the observations do not account for alongshore variability. Alongshore pressure gradients are an important component of the alongshore momentum balances at FRF and MVCO (Lentz et al., 1999; Fewings and Lentz, 2010), but observational estimates are not available concurrent with the observations presented in this study. Alongshore variations in velocity associated with three dimensional circulation patterns, which are neglected in the simplified momentum balance in equation (3), may also be significant. High-frequency radar observations of the surface circulation at MVCO suggest that momentum fluxes associated with lateral exchange can be important near complex bathymetry (Kirincich et al., 2013). Three dimensional processes may also affect the nonlinear momentum fluxes associated with two-dimensional upwelling and downwelling circulation patterns, which are the primary focus of this study. For example, Kumar and Feddersen (2017) show that including transient rip currents in a numerical model of circulation over a stratified inner shelf causes thermal wind balance to break down. Transient rip currents over the inner shelf may therefore influence the vertical shear of the alongshore flow, modulating the cross-shelf flux of alongshore momentum associated with upwelling and downwelling. Because nonlinear processes can significantly influence the alongshore momentum balance, studies of inner shelf dynamics should consider the potential for coupling between the dynamics of wind-driven circulation, submesoscale features and wave-driven flow over the inner shelf.

An implication of this study is that the cross-shelf wind stress can play a role in the

alongshore momentum balance. The cross-shelf wind stress increases surface transport U_s in shallow water, where alongshore wind stress is inefficient at driving cross-shelf exchange (Tilburg, 2003; Fewings et al., 2008). Increased surface transport increases the magnitude of the nonlinear momentum flux divergence relative to the wind stress in the scaling of the two terms in equation (14). However, cross-shelf wind stress alone does not drive significant alongshore flow (Tilburg, 2003), and therefore would not be expected to produce a strong momentum flux divergence. Combined offshore and upwelling-favorable wind stress, typical for the FRF site examined in this study, may provide optimal conditions for an important role of the nonlinear momentum flux divergence over the inner shelf.

6. Conclusion

The results of this study show that cross-shelf fluxes of alongshore momentum influence the physical dynamics of the inner shelf. The two locations examined contrast strongly in the circulation patterns associated with nonlinear momentum fluxes, and their overall importance in the alongshore momentum balance. Over the North Carolina inner shelf, the momentum flux divergence plays an important role in balancing the alongshore wind stress during upwelling-favorable and offshore winds. During reversals to downwelling-favorable and onshore forcing, the momentum flux divergence acts in the same direction as the wind stress, allowing bottom stress to exceed the wind stress. Over the New England inner shelf, the importance of the momentum flux divergence is reduced, and tends to act in opposition to both upwelling-favorable and downwelling-favorable wind stress. These differences over the New England inner shelf are consistent with a combination of weaker stratification, weaker vertical shear, a background mean upwelling circulation, and cross-shelf wind stress that tends counteract the surface transport driven by alongshore wind stress.

The role of the nonlinear momentum flux divergence should be taken into account at

inner shelf locations characterized by strong vertical shear and steep bottom slope. The mechanism described in this study is similar to that described by Lentz and Chapman (2004) for mid-shelf sites. However, the relationship between wind forcing, stratification, the cross-shelf density gradient, turbulent mixing and vertical shear is complex over the inner shelf. This complexity is not captured by a simple dependence on the slope Burger number. In addition, because cross-shelf winds influence transport in the surface layer, the cross-shelf component of wind stress has the potential to influence the alongshore momentum balance over the inner shelf. The dynamics of the shallow inner shelf are often characterized by an overall balance between wind stress and bottom stress. However, nonlinear momentum fluxes can either reduce or increase the role of bottom stress relative to the wind stress, which affects the relationship between mixing and exchange over the inner shelf.

Acknowledgments. We thank all of the scientists, engineers and technicians at Woods Hole Oceanographic Institution and the Army Corps of Engineers Field Research Facility who contributed to the collection of the time series data analyzed in this study. Current meter and water property data from the North Carolina inner shelf are publicly available at http://www.frf.usace.army.mil. Data are provided by the Field Research Facility, Coastal Observations & Analysis Branch, US Army Corps of Engineers, Duck, North Carolina. Support for this work was provided by the National Science Foundation (OCE-1433716 and OCE-1558874).

REFERENCES

Austin, J. A. 1999. The role of the alongshore wind stress in the heat budget of the North Carolina inner shelf. J. Geophys. Res. Ocean., *104*(C8), 18187–18203. doi: 10.1029/1998JC900122.

Austin, J. A. and S. J. Lentz. 1999. The relationship between synoptic weather systems and meteorological forcing on the North Carolina inner shelf. J. Geophys. Res. Ocean., *104*(C8), 159–185. doi: 10.1029/1999JC900016.

Austin, J. A. and S. J. Lentz. 2002. The inner shelf response to wind-driven upwelling and downwelling. J. Phys. Ocean., *32*(7), 2171–2193. doi: 10.1175/1520-0485(2002)032¡2171:TISRTW¿2.0.CO;2.

Castelao, R., R. Chant, S. Glenn, and O. Schofield. 2010. The effects of tides and oscillatory winds on the subtidal inner-shelf cross-shelf circulation. J. Phys. Oceanogr., *40* (4), 775–788. doi: 10.1175/2009JPO4273.1.

Chen, S.-Y. and S.-N. Chen. 2017. Generation of upwelling circulation under downwelling-favorable wind within bottom-attached, buoyant coastal currents. J. Phys. Oceanogr., *47*(10), 2499–2519. doi: 10.1175/JPO-D-16-0271.1.

Codiga, D. 2011. Unified tidal analysis and prediction using the UTide Matlab functions. Technical report, Graduate School of Oceanography, University of Rhode Island, Narragansett, RI. URL `http://www.po.gso.uri.edu/ codiga/utide/utide.htm`.

Cudaback, C. N. and J. L. Largier. 2001. The cross-shelf structure of wind- and buoyancy-driven circulation over the North Carolina inner shelf. Cont. Shelf Res., *21*(15), 1649–1668. doi: 10.1016/S0278-4343(01)00025-5.

Feddersen, F., R. T. Guza, S. Elgar, and T. H. C. Herbers. 1998. Alongshore momentum balances in the nearshore. J. Geophys. Res. Ocean., *103*(C8), 15667–15676. doi: 10.1029/98JC01270.

Fewings, M., S. J. Lentz, and J. Fredericks. 2008. Observations of cross-shelf flow driven by cross-shelf winds on the inner continental shelf. J. Phys. Oceanogr., *38*(11), 2358–2378. doi: 10.1175/2008JPO3990.1.

1107 Fewings, M. R. and S. J. Lentz. 2010. Momentum balances on the inner continental shelf
1108 at Martha's Vineyard Coastal Observatory. J. Geophys. Res. Ocean., *115*(12), C12023.
1109 doi: 10.1029/2009JC005578.

1110 Fewings, M. R. and S. J. Lentz. 2011. Summertime cooling of the shallow continental
1111 shelf. J. Geophys. Res. Ocean., *116*(C7). doi: 10.1029/2010JC006744.

1112 Ganju, N. K., S. J. Lentz, A. R. Kirincich, and J. T. Farrar. 2011. Complex mean circu-
1113 lation over the inner shelf south of Martha's Vineyard revealed by observations and a
1114 high-resolution model. J. Geophys. Res., *116*, C10036. doi: 10.1029/2011JC007035.

1115 Garvine, R. W. 2004. The vertical structure and subtidal dynamics of the inner shelf off
1116 New Jersey. J. Mar. Res., *62*(3), 337–371. doi: 10.1357/0022240041446182.

1117 Grifoll, M., A. L. Aretxabaleta, M. Espino, and J. C. Warner. 2012. Along-shelf current
1118 variability on the Catalan inner-shelf (NW Mediterranean). J. Geophys. Res. Ocean.,
1119 *117*(C9). doi: 10.1029/2012JC008182.

1120 Hickey, B. M. 1989. Patterns and processes of circulation over the Washington continental
1121 shelf and slope. In Landry, M. R. and B. M. Hickey, editors, *Coast. Oceanogr. Washingt.*
1122 *Oregon*, pages 41–115. Elsevier.

1123 Horwitz, R. and S. J. Lentz. 2014. Inner-shelf response to cross-shelf wind stress: The
1124 importance of the cross-shelf density gradient in an idealized numerical model and field
1125 observations. J. Phys. Oceanogr., *44*(1), 86–103. doi: 10.1175/JPO-D-13-075.1.

1126 Horwitz, R. M. and S. J. Lentz. 2016. The effect of wind direction on cross-shelf
1127 transport on an initially stratified inner shelf. J. Mar. Res., *74*, 201–227. doi:
1128 10.1357/002224016820870648.

1129 Kirincich, A. R. 2013. Long-term observations of turbulent Reynolds stresses over the
1130 inner continental shelf. J. Phys. Oceanogr., *43*(12), 2752–2771. doi: 10.1175/JPO-D-
1131 12-0153.1.

1132 Kirincich, A. R. and J. A. Barth. 2009a. Time-varying across-shelf Ekman transport and
1133 vertical eddy viscosity on the inner shelf. J. Phys. Oceanogr., *39*(3), 602–620. doi:
1134 10.1175/2008JPO3969.1.

1135 Kirincich, A. R. and J. A. Barth. 2009b. Alongshelf variability of inner-shelf circulation
1136 along the central Oregon coast during summer. J. Phys. Oceanogr., *39*(6), 1380–1398.
1137 doi: 10.1175/2008JPO3760.1.

1138 Kirincich, A. R., J. A. Barth, B. A. Grantham, B. A. Menge, and J. Lubchenco. 2005.
1139 Wind-driven inner-shelf circulation off central Oregon during summer. J. Geophys.
1140 Res., *110*(10), C10S03. doi: 10.1029/2004JC002611.

1141 Kirincich, A. R., S. J. Lentz, J. T. Farrar, and N. K. Ganju. 2013. The spatial structure
1142 of tidal and mean circulation over the inner shelf south of Martha's Vineyard, Mas-
1143 sachusetts. J. Phys. Oceanogr., *43*(9), 1940–1958. doi: 10.1175/JPO-D-13-020.1.

1144 Kuebel Cervantes, B. T., J. S. Allen, and R. M. Samelson. 2003. A modeling study of
1145 Eulerian and Lagrangian aspects of shelf circulation off Duck, North Carolina. J. Phys.
1146 Oceanogr., *33*(10), 2070–2092.

1147 Kuebel Cervantes, B. T., J. S. Allen, and R. M. Samelson. 2004. Lagrangian characteristics
1148 of continental shelf flows forced by periodic wind stress. Nonlinear Process. Geophys.,
1149 *11*(1), 3–16. doi: 10.5194/npg-11-3-2004.

1150 Kumar, N. and F. Feddersen. 2017. The effect of Stokes drift and transient rip currents
1151 on the inner shelf. Part II: With stratification. J. Phys. Oceanogr., *47*(1), 243–260. doi:
1152 10.1175/JPO-D-16-0077.1.

1153 Kumar, N., G. Voulgaris, J. C. Warner, and M. Olabarrieta. 2012. Implementation of
1154 the vortex force formalism in the coupled ocean-atmosphere-wave-sediment transport
1155 (COAWST) modeling system for inner shelf and surf zone applications. Ocean Model.,
1156 *47*, 65–95. doi: 10.1016/j.ocemod.2012.01.003.

1157 Lee, G.-h., C. T. Friedrichs, and C. E. Vincent. 2002. Examination of diffusion ver-
1158 sus advection dominated sediment suspension on the inner shelf under storm and
1159 swell conditions, Duck, North Carolina. J. Geophys. Res., *107*(C7), 3084. doi:
1160 10.1029/2001JC000918.

1161 Lentz, S. J. 1995. Sensitivity of the inner-shelf circulation to the form of the eddy viscosity
1162 profile. J. Phys. Oceanogr., *25*, 19–28.

1163 Lentz, S. J. 2008a. Seasonal variations in the circulation over the Middle Atlantic Bight
1164 continental shelf. J. Phys. Oceanogr., *38*, 1486–1500. doi: 10.1175/2007JPO3767.1.

1165 Lentz, S., R. T. Guza, S. Elgar, F. Feddersen, and T. H. C. Herbers. 1999. Momentum
1166 balances on the North Carolina inner shelf. J. Geophys. Res., *104*(C8), 18205–18226.
1167 doi: 10.1029/1999JC900101.

1168 Lentz, S. J. 2001. The influence of stratification on the wind-driven cross-shelf cir-
1169 culation over the North Carolina shelf. J. Phys. Oceanogr., *31*(9), 2749–2760. doi:
1170 10.1175/1520-0485(2001)031¡2749:TIOSOT¿2.0.CO;2.

1171 Lentz, S. J. 2008b. Observations and a model of the mean circulation over the
1172 Middle Atlantic Bight continental shelf. J. Phys. Oceanogr., *38*, 1203–1221. doi:
1173 10.1175/2007JPO3768.1.

1174 Lentz, S. J. and D. C. Chapman. 2004. The importance of nonlinear cross-shelf momentum
1175 flux during wind-driven coastal upwelling. J. Phys. Oceanogr., *34*(11), 2444–2457. doi:
1176 10.1175/JPO2644.1.

1177 Lentz, S. J. and M. R. Fewings. 2012. The wind- and wave-driven inner-shelf circulation.
1178 Ann. Rev. Mar. Sci., *4*, 317–343. doi: 10.1146/annurev-marine-120709-142745.

1179 Lentz, S. J. and J. Largier. 2006. The influence of wind forcing on the Chesa-
1180 peake Bay buoyant coastal current. J. Phys. Oceanogr., *36*(2005), 1305–1316. doi:
1181 10.1175/JPO2909.1.

Lentz, S. J., M. Fewings, P. Howd, J. Fredericks, and K. Hathaway. 2008. Observations and a model of undertow over the inner continental shelf. J. Phys. Oceanogr., *38*(11), 2341–2357. doi: 10.1175/2008JPO3986.1.

Li, Z. and R. H. Weisberg. 1999. West Florida continental shelf response to upwelling favorable wind forcing 2. Dynamics. J. Geophys. Res., *104*(C10), 23427–23442.

Liu, Y. and R. H. Weisberg. 2005. Momentum balance diagnoses for the West Florida Shelf. Cont. Shelf Res., *25*(17), 2054–2074. doi: 10.1016/j.csr.2005.03.004.

Mazzini, P. L., R. J. Chant, M. E. Scully, J. Wilkin, E. J. Hunter, and N. J. Nidzieko. 2019. The impact of wind forcing on the thermal wind shear of a river plume. J. Geophys. Res. Ocean., *124*(11), 7908–7925. doi: 10.1029/2019JC015259.

Mitchum, G. T. and A. J. Clarke. 1986. The frictional nearshore response to forcing by synoptic scale winds. J. Phys. Oceanogr., *16*(5), 934–946.

Monismith, S. G. and D. A. Fong. 2004. A note on the potential transport of scalars and organisms by surface waves. Limnol. Ocean., *49*(4), 1214–1217. doi: 10.4319/lo.2004.49.4.1214.

Moody, J. A., B. Butman, R. C. Beardsley, W. S. Brown, P. Daifuku, J. D. Irish, D. A. Mayer, H. O. Mofjeld, B. Petrie, S. Ramp, P. Smith, and W. R. Wright. 1984. Atlas of tidal elevation and current observations on the Northeast American continental shelf and slope. Bulletin 1611. Technical report, U.S. Geological Survey. URL `http://pubs.er.usgs.gov/publication/b1611`.

Ofsthun, C., X. Wu, G. Voulgaris, and J. C. Warner. 2019. Alongshore momentum balance over shoreface-connected ridges, Fire Island, NY. Cont. Shelf Res. doi: 10.1016/j.csr.2019.07.005.

1205 Rennie, S. E., J. L. Largier, and S. J. Lentz. 1999. Observations of a pulsed buoy-
1206 ancy current downstream of Chesapeake Bay. J. Geophys. Res., *104*(C8), 18227. doi:
1207 10.1029/1999JC900153.

1208 Rosenfeld, L. K. 1983. CODE-1: Moored array and large-scale data report, Technical
1209 Report 83-23, Woods Hole Oceanographic Institution. Technical report, Woods Hole
1210 Oceanographic Institution.

1211 Smith, J. A. 2006. Wave-current interactions in finite depth. J. Phys. Oceanogr., *36*(7),
1212 1403–1419. doi: 10.1175/JPO2911.1.

1213 Smith, S. D. 1988. Coefficients for sea surface wind stress, heat flux, and wind profiles as
1214 a function of wind speed and temperature. J. Geophys. Res. Ocean., *93*(C12), 15467–
1215 15472. doi: 10.1029/JC093iC12p15467.

1216 Thieler, E., D. Foster, D. Mallinson, E. Himmelstoss, J. McNinch, J. List, and E. Hammar-
1217 Klose. 2013. Quaternary geophysical framework of the northeastern North Car-
1218 olina coastal system: U.S. Geological Survey Open-File Report 2011-2015. URL
1219 `https://pubs.usgs.gov/of/2011/1015/`.

1220 Tilburg, C. E. 2003. Across-shelf transport on a continental shelf: Do across-shelf winds
1221 matter? J. Phys. Oceanogr., *33*(12), 2675–2688.

1222 Uchiyama, Y., J. C. McWilliams, and A. F. Shchepetkin. 2010. Wave-current interaction
1223 in an oceanic circulation model with a vortex-force formalism: Application to the surf
1224 zone. Ocean Model., *34*, 16–35. doi: 10.1016/j.ocemod.2010.04.002.

1225 Weisberg, R. H., Z. Li, and F. Muller-Karger. 2001. West Florida shelf response to local
1226 wind forcing: April 1998. J. Geophys. Res. Ocean., *106*(C12), 31239–31262. doi:
1227 10.1029/2000JC000529.

1228 Woodson, C. B. 2013. Spatiotemporal variation in cross-shelf exchange across the
1229 inner shelf of Monterey Bay, California. J. Phys. Ocean., *43*(8), 1648–1665. doi:
1230 10.1175/JPO-D-11-0185.1.

1231 Xu, F.-H. and L.-Y. Oey. 2011. The origin of along-shelf pressure gradient in the Middle
1232 Atlantic Bight. J. Phys. Oceanogr., *41*(9), 1720–1740. doi: 10.1175/2011JPO4589.1.

1233 Xu, Z. and A. J. Bowen. 1994. Wave- and wind-driven flow in water of finite depth. J.
1234 Phys. Ocean., *24*, 1850–1866.

Table 1: Results from piecewise linear regressions between wind stress and nonlinear terms in the depth averaged momentum balance over the North Carolina inner shelf during June-August. Analysis is restricted to time periods when each site is outside the surf zone and $\bar{u}_L < 0.03$ m/s. Regression slopes are given with 95% confidence intervals for both upwelling favorable wind stress (positive τ^{sy}) and downwelling favorable wind stress (negative τ^{sy}) at five different pairs of sites. Results from the 6m-8m sites are shown in Figure 6.

Sites	Upwelling favorable	Downwelling favorable
5m-6m	0.51 ± 0.5	-0.15 ± 0.6
5m-8m	0.5 ± 0.21	-0.38 ± 0.22
6m-8m	0.57 ± 0.21	-0.77 ± 0.51
6m-11m	0.87 ± 0.32	-0.46 ± 0.36
8m-11m	0.66 ± 0.4	-0.32 ± 0.33

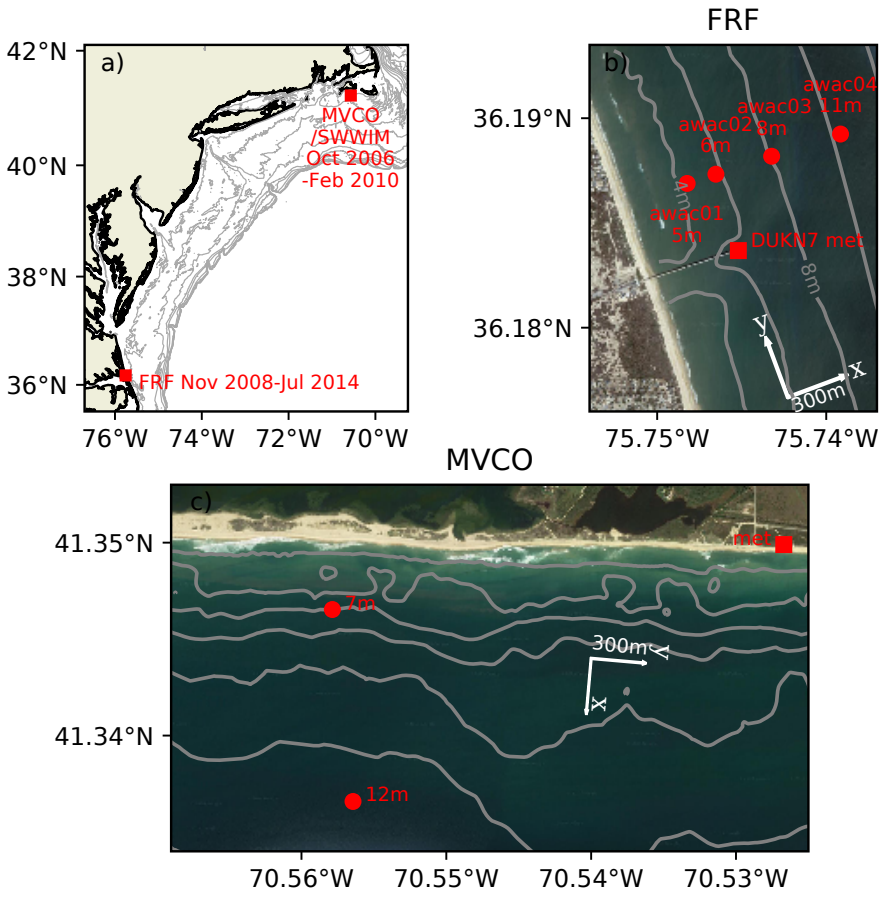

Figure 1: a) Coastline and bathymetry of the Mid-Atlantic Bight region. Red squares indicate locations of long-term current meter arrays used in this study. Red triangle indicates location of long-term tide gauge at the mouth of Chesapeake Bay. Gray contours indicate isobaths at 20-m intervals out to 200 m. b) Overview of FRF field site at Duck, NC, showing locations of current meters (circles), tide gauge (triangle) and meteorological observations (square). Contours indicate isobaths at 2 m intervals, starting at the 4 m isobath. Axes show average offshore (x) and upwelling-favorable (y) coordinate system orientation determined from principal axis analyses of current meter data. Length of arrows depicts horizontal scale of 300 m. c) Overview of MVCO field site at Martha's Vineyard, MA, showing locations of current meters at the 7 m and 12 m isobaths from the SWWIM project (circles) and MVCO beach meteorological observations (square). Contours indicate isobaths at 2 m intervals, starting at the 2m isobath. Coordinate system and scales as in panel b.

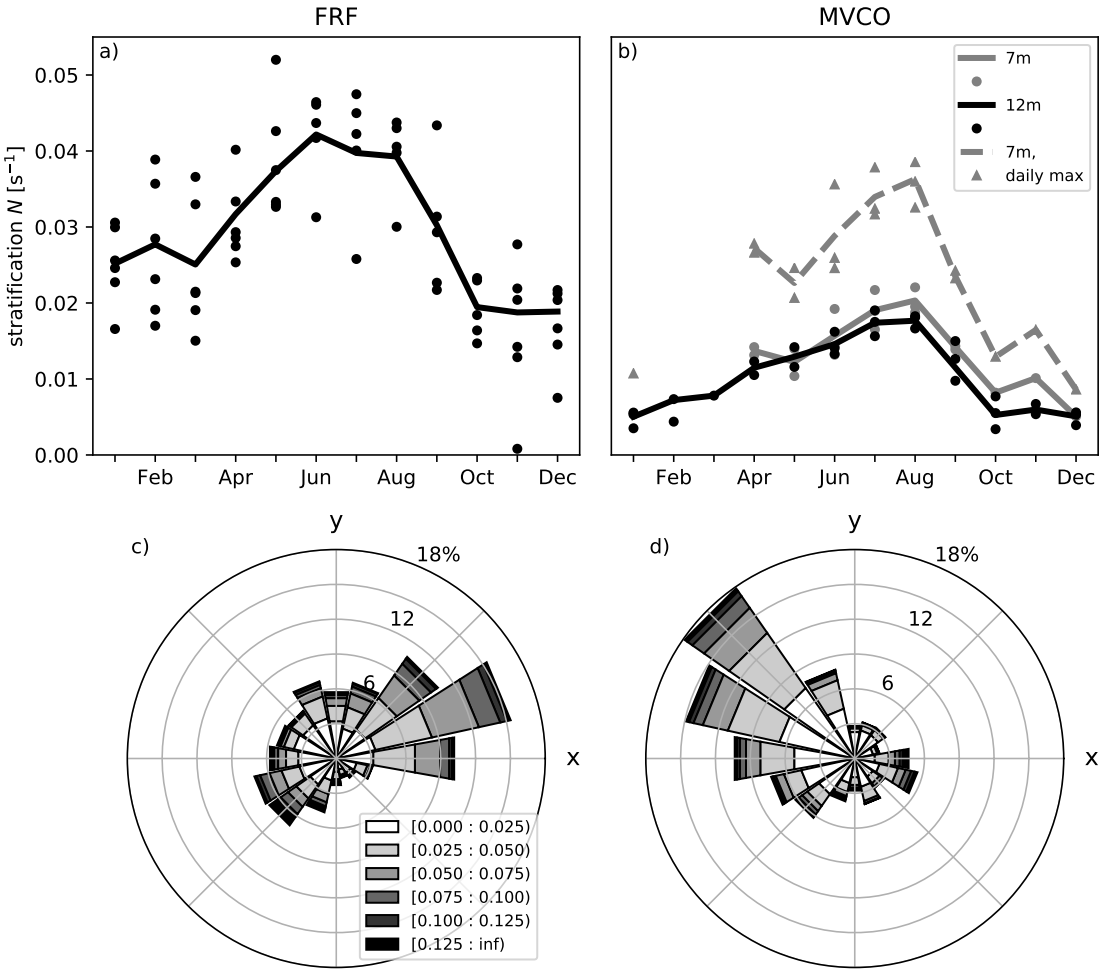

Figure 2: Comparison of stratification (a, b) and wind stress (c,d) at the FRF site in Duck, NC (left column) and Martha's Vineyard, MA (right column). a) Monthly averages of buoyancy frequency, N, calculated from daily vertical profiles at the end of the FRF pier (black circles). Line shows seasonal climatology computed from monthly averages. b) Monthly averages and seasonal climatology of N computed from all SWWIM mooring observations at the 7 m site (gray circles and solid line) and 12 m site (black circles and solid line). Monthly averages and climatology of N computed from daily maxima at the 7 m site are also shown (gray triangles and dashed line). c) Wind rose plot for FRF site, showing frequency of occurrence of wind stress magnitude (N/m^2) and direction at FRF site during the months of June-August. The coordinate system has been rotated relative to offshore (x) and upwelling-favorable (y) coordinates shown in Figure 1b. d) As in panel c, for MVCO site and coordinate system shown in Figure 1c.

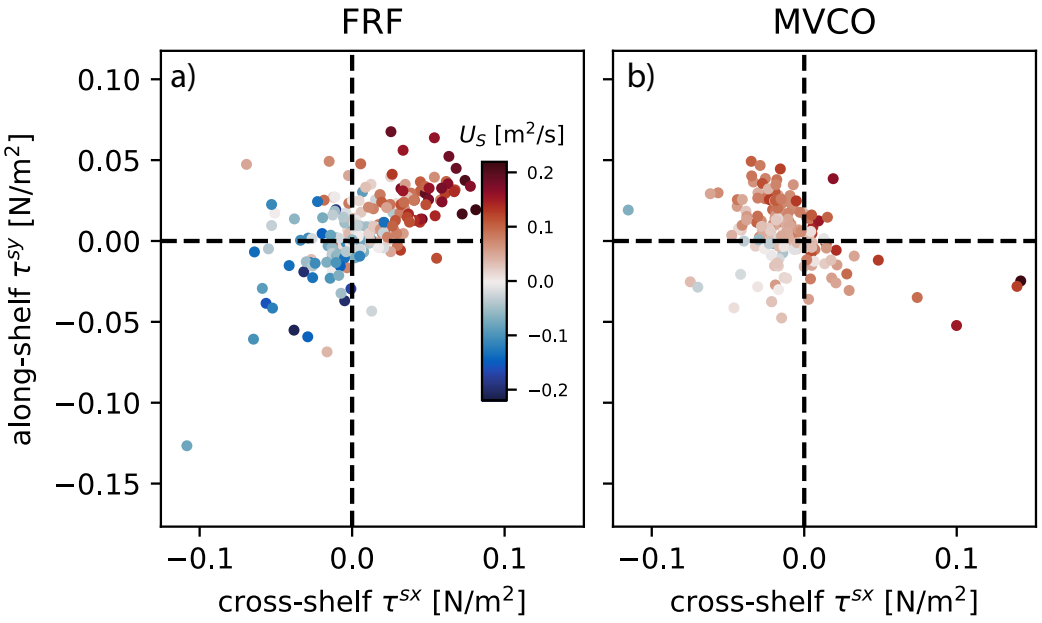

Figure 3: Cross-shelf and along-shelf components of wind stress (τ^{sx},τ^{sy}) during the months of June-August, with colors indicating surface transport U_s at a) FRF, and b) MVCO. Each point represents a 33-hour average of low-pass filtered data.

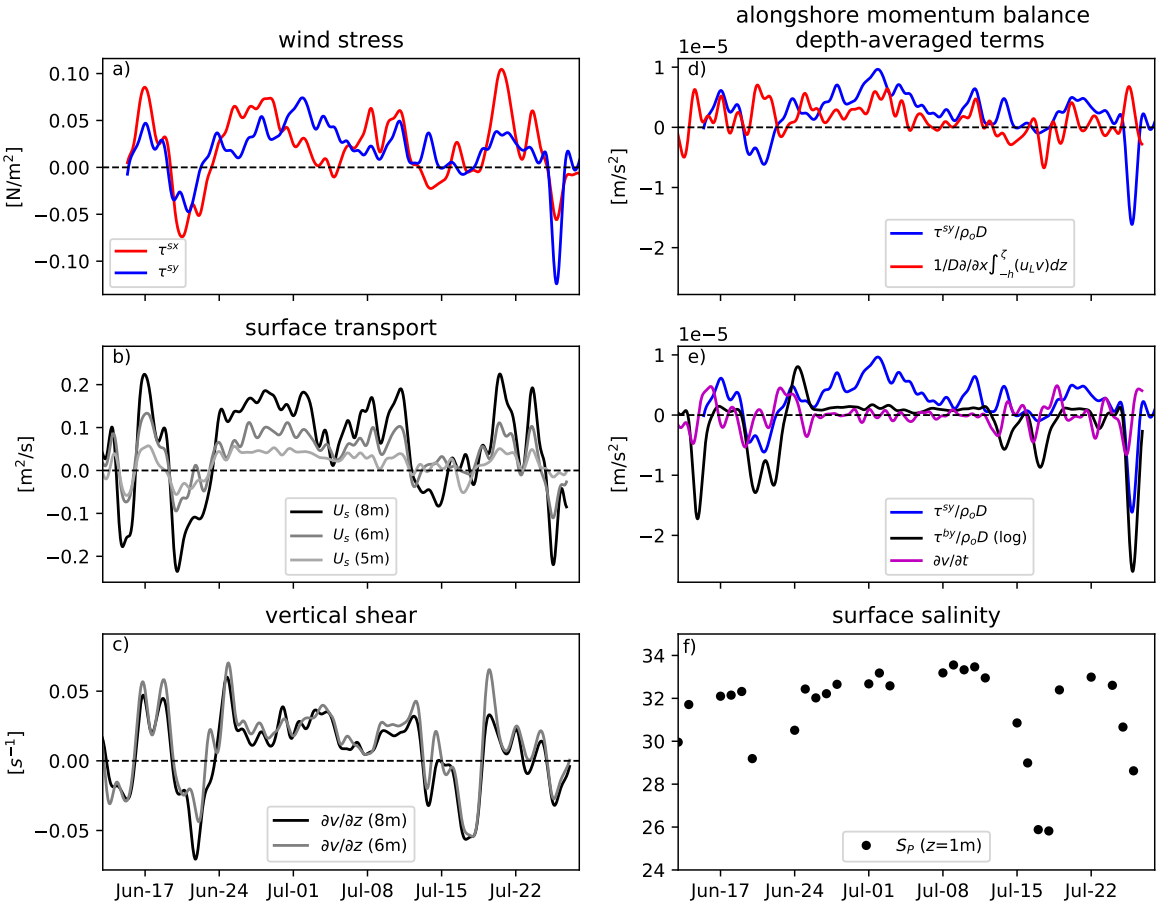

Figure 4: Time series at FRF during the 45-day period 13 June–28 July 2013. a) Cross-shore (red) and alongshore (blue) components of wind stress. b) Cross-shore surface transport, U_S, at the 8 m (black), 6 m (dark gray) and 5 m (light gray) sites. c) Vertical shear in alongshore currents, $\partial v/\partial z$, at the 8 m site. d) Selected terms in the depth-integrated alongshore momentum balance, averaged between the 6 m and 8 m sites: wind stress ($\tau^{sy}/\rho_o D$, blue) and nonlinear advection ($1/D\partial/\partial x \int_{-h}^{\eta}(u_L v)dz$, red). e) Selected terms in the depth-integrated alongshore momentum balance, averaged between the 6 m and 8 m sites: wind stress ($\tau^{sy}/\rho_o D$, blue) and linearized bottom stress ($\tau^{by}/\rho_o D$, black). f) Practical salinity, S_P, from CTD casts at a depth of 1 m.

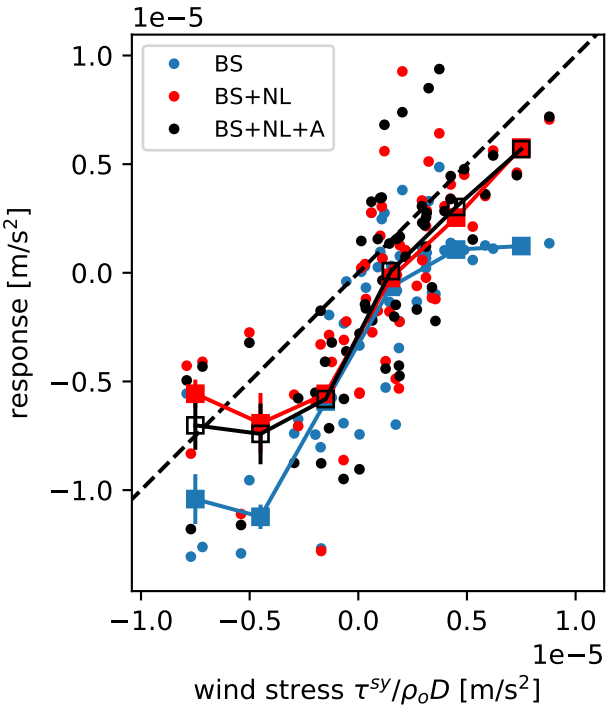

Figure 5: Comparison of wind stress, bottom stress and nonlinear advection terms in the depth-averaged alongshore momentum balance at FRF during June–August. Wind stress term vs. bottom stress (BS) term (blue); wind stress term vs. sum of bottom stress and nonlinear (BS + NL) terms (red); and wind stress term vs. sum of bottom stress, nonlinear and acceleration (BS + NL + A) terms (black). Each circle represents a 33-hour average of low-pass filtered data. Squares are bin averages, with vertical lines showing standard errors.

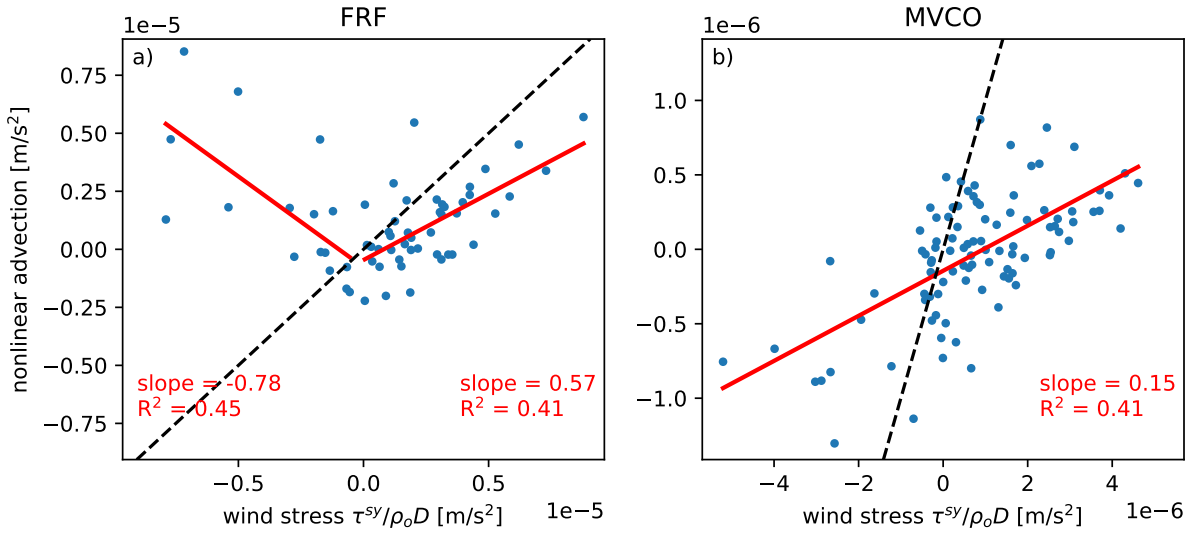

Figure 6: Comparison of wind stress and nonlinear advection terms in the alongshore momentum balance during June–August. a) At FRF over the North Carolina inner shelf. Red lines indicate results of piecewise linear regressions of the 33-hour subsampled values, one regression for positive values of wind stress and another for negative values of wind stress. b) At MVCO over the New England inner shelf. One linear regression is used for both positive and negative values of wind stress. Note difference in scale between panels a and b.

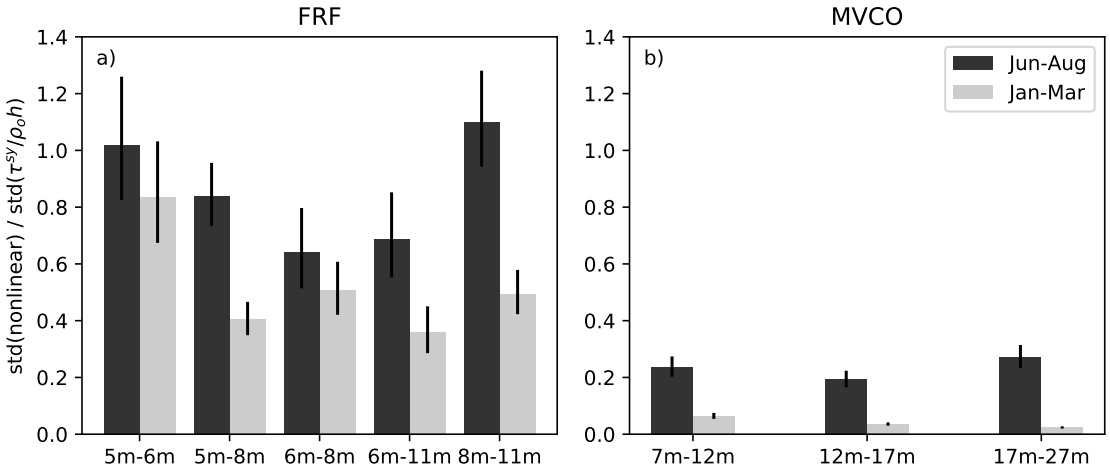

Figure 7: Comparison of variability in the nonlinear and wind stress terms in the alongshore momentum balance. a). Ratio of standard deviations of the nonlinear term and wind stress term at FRF over the North Carolina inner shelf. Black bars show ratios during June–August and gray bars show ratios during January–February. Ratios are shown for five different pairs of sites. Vertical lines indicate 95% confidence intervals. b) As in panel a, for three pairs of sites at MVCO over the New England inner shelf.

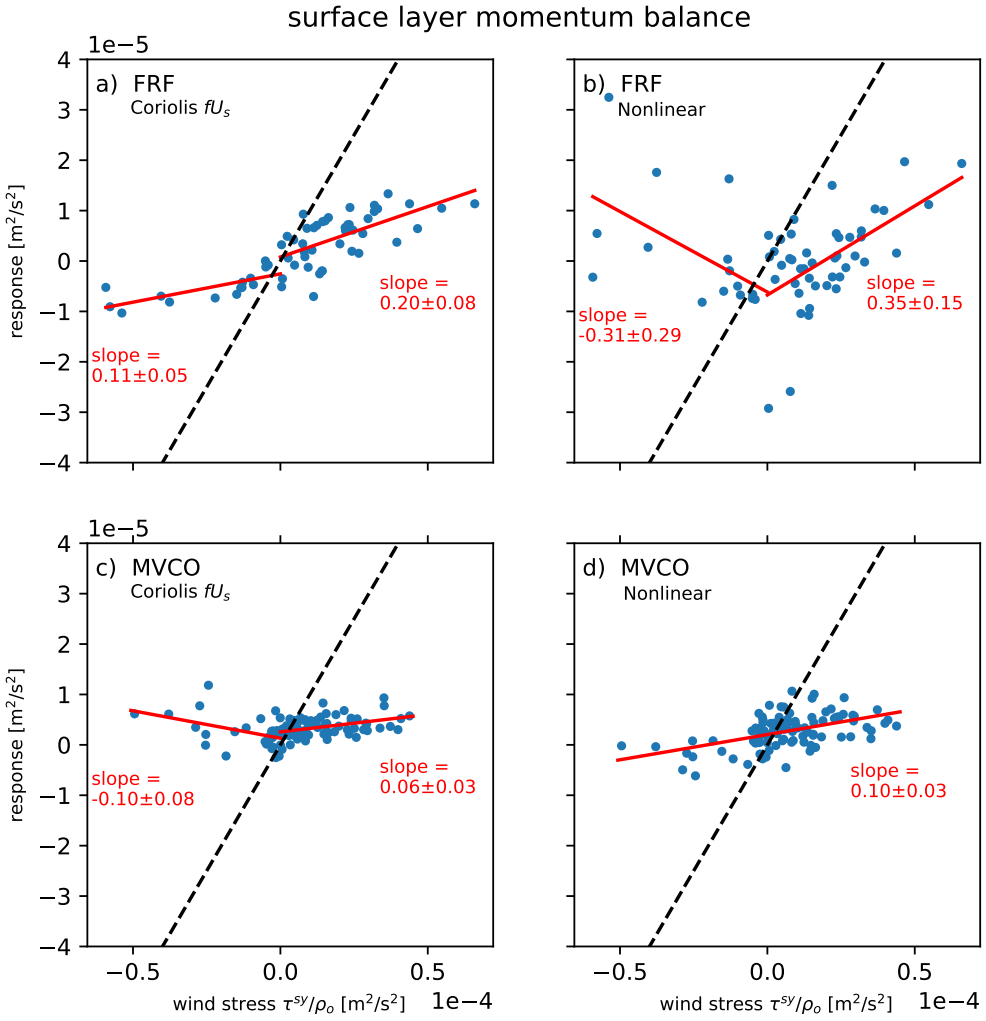

Figure 8: Comparison of wind stress, Coriolis and nonlinear advection terms in the surface layer-integrated alongshore momentum balance at FRF during June–August. a) Wind stress term vs. Coriolis terms at FRF. Each circle indicates a 33-hour average of low-pass filtered data. Lines indicate separate linear regression fits for positive and negative wind stress values. Regression slopes are shown with 95% confidence intervals. b) As in panel a, for wind stress term vs. nonlinear terms at FRF. c) As in panel a, for wind stress term vs. Coriolis term at MVCO. d) As in panel a, for wind stress term vs. nonlinear terms at MVCO, and with one linear regression fit for all data points.

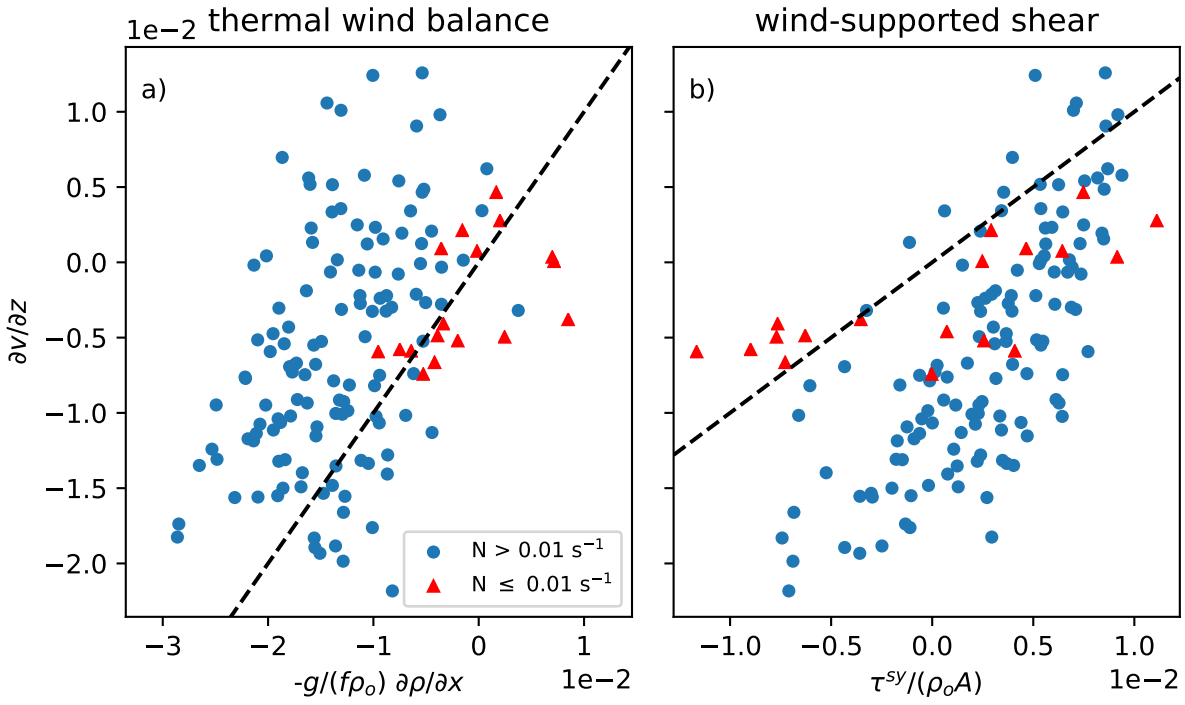

Figure 9: Evaluation of processes governing vertical shear, $\partial v/\partial z$, at MVCO. a) Hypothetical vertical shear associated with thermal wind balance in equation (7). Circles indicate relatively strong stratification, $N > 0.01$. Triangles indicate relatively weak stratification, $N \leq 0.01$. Black dashed line indicates 1:1 relationship. b) Hypothetical vertical shear associated with alongshore wind stress τ^{sy} and eddy viscosity $A = \kappa u_* h/6$ in equation (8).

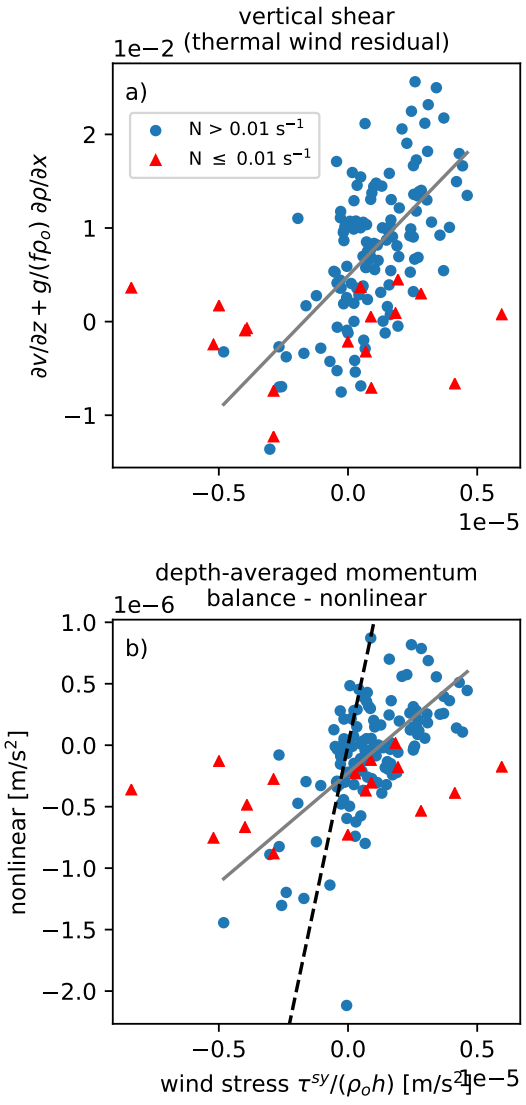

Figure 10: a) Wind stress term $\tau^{sy}/(\rho_o h)$ vs. the thermal wind balance residual $\partial v/\partial z + g/(f\rho_o)\partial\rho/\partial x$ at MVCO. Circles indicate relatively strong stratification, $N > 0.01$. Triangles indicate relatively weak stratification, $N \leq 0.01$. b) Wind stress and nonlinear advection terms in the depth-averaged momentum balance at MVCO under different levels of stratification.

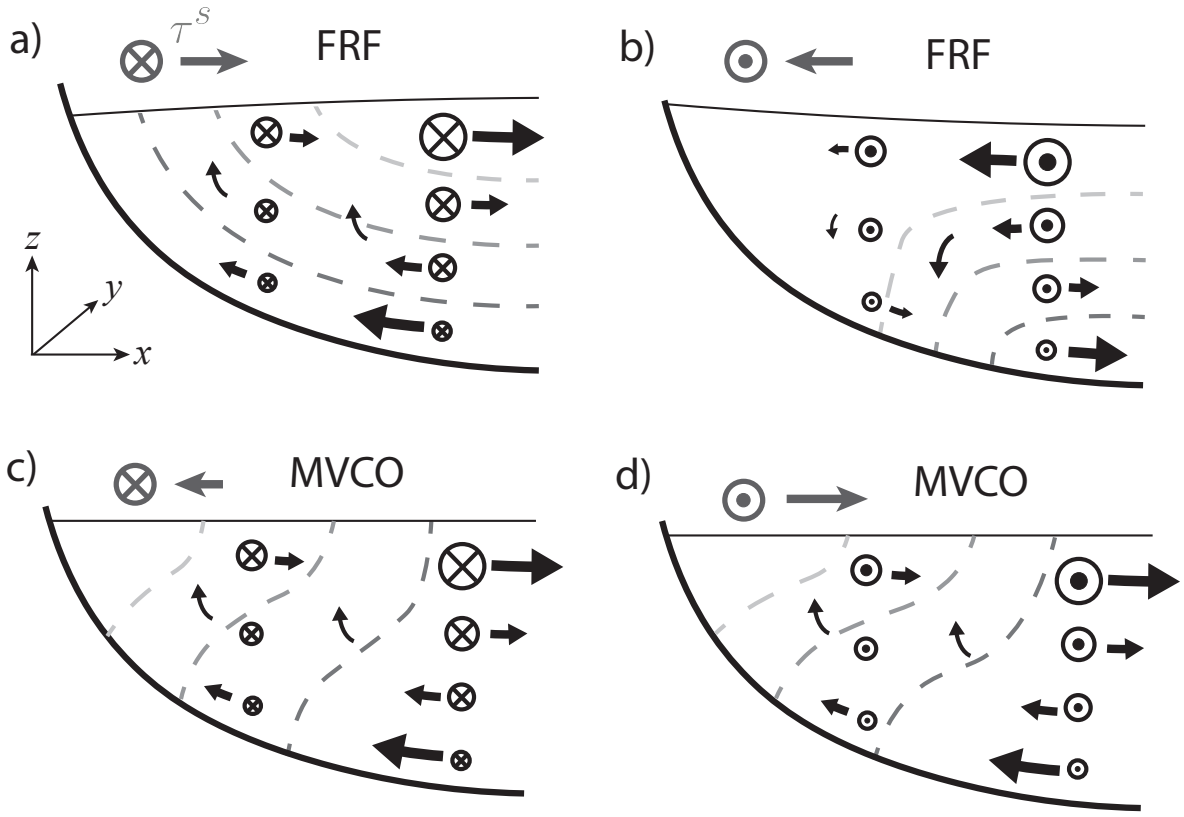

Figure 11: Conceptual models of circulation patterns associated with nonlinear momentum fluxes at different locations and under different forcing conditions. Arrows represent cross-shelf and vertical vector components. Circles represent alongshore vector components ($\otimes$ indicates wind stress or ocean velocity in the positive y direction). Dashed lines indicate isopycnals, where darker shading is relatively dense. a) FRF, upwelling-favorable and offshore wind stress. b) FRF, downwelling-favorable and onshore wind stress. c) MVCO, upwelling-favorable and onshore wind stress. d) MVCO, downwelling-favorable and offshore wind stress.

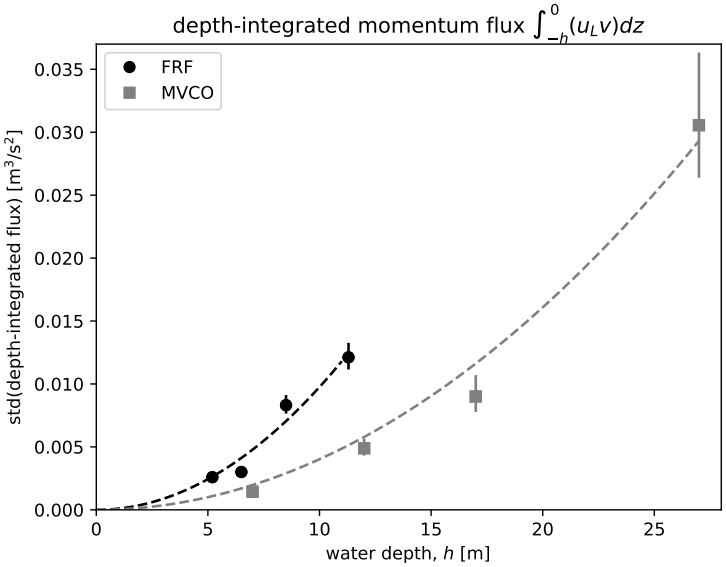

Figure 12: Standard deviations of the depth-integrated nonlinear momentum flux as a function of water depth, for the months of June–August. Black symbols represent estimates from FRF and gray symbols represent estimates from MVCO. Vertical bars indicate 95% confidence intervals. Dashed lines show hypothetical dependence on ah^2, where a is a constant coefficient obtained from a least squares fit at each location.

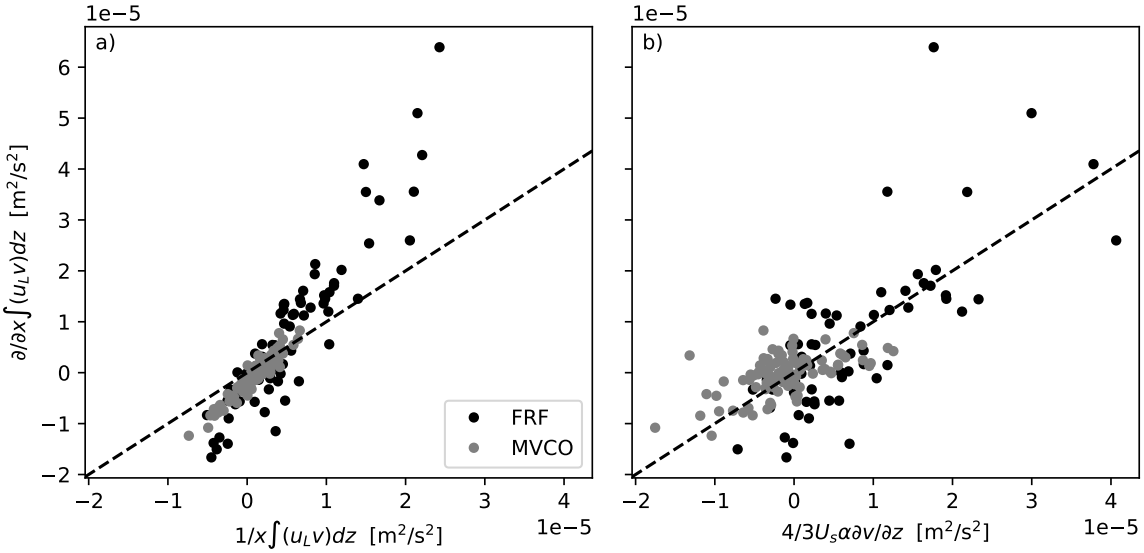

Figure 13: Simplified representations of the nonlinear term in the depth-averaged momentum balance. a) Comparison of the approximation in equation (9) estimated from single deeper mooring (x-axis) vs. full estimate from mooring pairs (y-axis). Black symbols represent estimates from the 6–8m sites at FRF and gray symbols represent estimates from the 7–12m sites at MVCO. Blacked dashed line represents 1:1 agreement. b) Comparison of the scaling in equation (12) estimated from single deeper mooring (x-axis) vs. full estimate from mooring pairs (y-axis). Symbols as in panel a.